

Dear Editor,

We are indeed grateful to the reviewers for their insights and critiques. The following is our point-to-point response to their questions (with line number in the manuscript if any). The comparison between the original and the revised manuscript is provided in a separate file.

With best regards,

Jane Liu

Review 1:

1. p. 28024, l. 19. The word 'contaminated' or 'contamination' (also appearing on p. 28029, l. 24; on p. 28046, l. 7; and on p. 28049, l. 12) does not seem like the best choice here; the actual point seems to be that the MOPITT vertical resolution is typically quite coarse. This is typical for satellite remote sensing products and is well understood by most users of MOPITT data. MOPITT and other CO-measuring satellite instruments cannot directly measure the volume mixing ratio at a specific pressure level, but they can accurately measure average mixing ratio over a thick layer.

Thanks for the points. These points are described in Discussion (L768-711). Word "contamination" is not used.

2. p. 28025, l. 17. The meaning of '... a swath of 29 pixels ...' is not clear. One cross-track scan of the MOPITT instrument actually generates $29 \times 4 = 116$ pixels.

Thanks. "4 pixels in a row" is added (L140).

3. p. 28025, l. 21. The meaning of 'complete global coverage' is not clear, since persistently cloudy areas (such as areas of the Amazon Basin) might not be observed at all in a continuous period of 16 days. Is there a reference for this statement regarding complete global coverage?

The phrase is removed.

4. p. 28026, l. 6. In addition to the MOPITT version number, this paragraph should state which level of MOPITT data was used. Level 2 (individual retrievals) or Level 3 (gridded)?

"Level 2" is added (L158).

5. p. 28024, l. 23. Add reference to MOPITT Version 5 validation paper (Deeter, M. N., et al (2013), Validation of MOPITT Version 5 thermal-infrared, near-infrared, and multispectral carbon monoxide profile retrievals for 2000–2011, J. Geophys. Res., doi:10.1002/jgrd.50272).

This reference is added (L991) and discussed in this revision (L300-306).

6. p. 28026, l. 4. Since MOPITT V5 data are used extensively in this paper, there should be some discussion of (and reference to) the results presented in the MOPITT V5 validation paper. For example, results in that paper indicate a retrieval bias in the upper troposphere. Would that explain some of the features of the MOPITT/MOZAIC comparisons shown in Fig. 2?

Yes, Deeter et al. (2013) compared MOPITT data with the NOAA aircraft measurements over North America and data from the HIAPER Pole to Pole Observations (HIPPO) field campaign data (Wofsy et al., 2011). They found a positive bias in MOPITT V5 TIR/NIR data at 400 hPa (4%) and 200 hPa (14%). They also showed a latitude-dependent positive bias in the northern hemispherical upper troposphere in MOPITT V3 and V4 data. This study suggests an overall positive bias in the upper troposphere, agreeing with Deeter et al. (2013) in magnitude and sign, in MOPITT V5 data. We have added the discussion for Fig. 2 (L300-306).

7. p. 28026, l. 19. Important details seem to be missing in this section (and in the captions to Figures 2 and 3) concerning the method used to identify MOPITT observations corresponding to a particular MOZAIC flight. MOZAIC vertical 'profiles' are actually produced by observations made over a slant path with varying latitude and longitude. For each MOZAIC flight, was the MOPITT collocation radius (1.5 degrees) applied to a single MOZAIC lat/lon location at a specific altitude or to all of the MOZAIC lat/lon values within some altitude range? Also, are the results presented in Figures 2 and 3 sensitive to the chosen collocation radius?

The radius of 1.5° is applied to a selected MOZAIC profile at 500 hPa so that the MOZAIC slant path can be included. Only when the entire slant path is within the radius, the MOZAIC profile is selected (L171-172). Because of adequate MOPITT samplings in the radius, the results in Figures 2 and 3 are not affected much by slight change in radius.

8. p. 28032, l. 22. The meaning of 'some degree of vertical sensitivity' is unclear. Does this statement refer to the ability to detect enhanced CO at a particular level, or to the vertical resolution?

We clarified this in this version of the manuscript. The vertical sensitivity is demonstrated through (1) the strongest CO source among the three cases was captured by the largest magnitude of CO enhancement of 200-250 ppbv from the a priori, (2) the altitude of the maximum CO enhancement was detected around the middle troposphere, in contrast to the other two cases which show the maximum in the lower-middle and upper troposphere, respectively, and (3) the elevated CO was over a broad range of altitudes as the vertical resolution of MOPITT is rather coarse, i.e., the maximum DFS is about 2.5 (Figure 1) (L348-354).

9. For all case studies, what criteria were used to determine the locations and shapes of the MOPITT boxes shown in Figure 4 determined?

The criteria are to ensure enough samplings of MOPITT measurements (no less than 30 data points) at the closest upwind direction of MOZAIC measurements. We have explained this in the caption (L1384-1385).

10. p. 28046, l. 5. Suggest replacing 'smooth MOZAIC profiles' with 'averaging kernel smoothed MOZAIC profiles.'

Changed (L783).

11. p. 28047, l. 16. 'MOPITT satellite' should be 'MOPITT satellite instrument'.

Changed (L810).

12. p. 28048, l. 17. 'frontal activates' should be 'frontal activity'

Corrected (L842).

13. p. 28049, l. 19. The last sentence of the Conclusion is unclear and seems to imply a bias in the MOPITT data. The statement 'MOPITT substantially underestimates CO in high CO episodes' really seems to be referring to the fact that remote sensing instruments like MOPITT cannot resolve sharp peaks in the CO profile. This is an issue of vertical resolution and does not imply a bias.

This sentence is removed.

14. p. 28066, Fig. 4. In addition to showing the location of the airport in each panel as an indicator of the location of the MOZAIC profile (i.e., the red dots), the figure should show a series of points indicating the actual latitude and longitude of the MOZAIC data at various altitudes or pressures (e.g., at 1 km or 100 hPa intervals).

Thanks for the suggestion. The geographic locations of MOZAIC data at 900, 600 and 300 hPa are now added in Figure 4.

15. p. 28073, Fig. 11. In this figure, why does latitude decrease from left to right? This will certainly confuse most readers.

Figure 11 and Figure 6 are re-plotted with increasing latitude from left to right.

Review 2:

One thing that wasn't clear to me is how frequent are these episodes of enhanced vertical transport. The authors identify just 3 cases across several years. Are these episodes hard to spot in the sparse data? Very infrequent? If the latter, do they add up to an important contribution regionally? world-wide? Does the model see more of them? Or are they a case study to more easily learn about vertical transport? It would be very useful to read more background.

Thanks for the points. More background information is now provided and discussed in Sect. 5.1 (L663-688). The frequency of high CO episodes observed by MOZAIC around Narita was summarized in original Table 2. The frequency of high CO episodes appeared in MOPITT and GEOS-Chem data is provided in a new Table 3. According to these data, it is likely that the high CO episodes shown in this study occurred 2-4 times every 100 days for each lower, middle and upper troposphere over the Sea of Japan and the East China Sea. GEOS-Chem does not see more high CO episodes in the free troposphere than MOZAIC or MOPITT. Overall, MOZAIC observed slightly more transport of high CO to the upper troposphere, while GEOS-Chem simulates more transport of CO (with lower abundances) to the middle and lower troposphere. According to Tables 2 and 3, air mass with 200-300 ppbv CO is transported to 400-200 hPa at a frequency of 10-20 times per 100 days, or approximately once a week. This can have significant impacts on the air quality downwind. The transport mechanisms and CO source contributions revealed in this study can also be applicable for these CO episodes, even at lower CO abundances or lower altitudes (L663-688).

In general, I think the sections should be shortened and made more concise, especially given the lack of quantitative information. The authors are strongly encouraged to add quantitative information.

The contents in the original Sect.5 (Discussion) are substantially removed. We have added more quantitative information in Discussion and in Table 3.

p28025, l 5-10. It's a bit confusing to read about demonstrating MOPITT's vertical sensitivity, since I thought it was MOPITT's vertical sensitivity that was being used to evaluate the vertical transport, not the other way around. It would be great to be clear about that here already.

MOPITT data are analyzed in two ways in this study. First, the vertical sensitivity of MOPITT is evaluated with the coincident MOZAIC data (see Figures 1, 2 and 3) and further illustrated with in the high CO episodes in comparison with the MOZAIC data (see Figure 5). Second, the vertical variation in CO captured by MOPITT is used to diagnose vertical transport of CO (Figure 6) (L125-131).

p28027, l 17-19. It would be great to put the list of parameters at the beginning of this subsection, otherwise, it's a bit unclear what "analyses" include Section 2.5 Are the met data described in 2.3 used only to drive FLEXPART? Perhaps it's better to combine those two sections then, similarly to how GMAO met fields are in the same section as GEOS-Chem Section 2.6.

The list of parameters is moved to the beginning of this section. We added "In addition to driving FLEXPART, the FNL data are used to analyze the meteorological conditions including the surface pressure, wind fields, and development of a cyclone." (L208-210). We moved this section right ahead of

the section on FLEXPART.

Is the full chemistry version of GEOS-Chem being used as implied or is it just tagged CO/single tracer simulation?

GEOS-Chem was used in the full chemistry mode. This information is added into the text (L234).

p.28030, l20-21. I don't understand the concept of "difference between averaging kernels", is it its diagonals?

The difference is the averaging kernel for each retrieved pressure level between version 5 and version 4.

Section 4.1 It's an interesting reconstruction of the history of a pollution plume, but I'm not sure how much of this was not known before. It's not clear what's new here. Is it that pollution is transported via WCB? That it is lofted 9 km? That it reaches Canada? That MOPITT and models agree? None of this sounds new, so it would be helpful if the authors stated more explicitly what new insights they have gained here. I'm also curious what does GEOS-Chem say about this case study.

Thanks for the comments. New insights gained from this case are now discussed at the end of Sect. 4.1 (L417-422). More detail on GEOS-Chem simulation for this case is provided in Sect. 5.5 (L743-745).

p28036, l2. "This source is confirmed in the GEOS-Chem simulation". Are the authors really relying more on GEOS-Chem than MOPITT to confirm cases of vertical transport of pollution? Shouldn't it be the other way around? especially at 700hPa. Naturally, it would be good to have independent data set here, but I guess MOZAIC was not available? It would be good if the sections were a bit more parallel (each commenting on the skill of both models and availability and quality of both data sets) Is Figure 12 necessary?

Thanks for the points. This study aims for solving puzzles of vertical transport of CO, using observations from MOZAIC and MOPITT and simulations from FLEXPART and GEOS-Chem, as well as other data. All the data and simulations were integrated to examine if they support or complement each other without particular preference to one dataset or simulation. In this case, elevated CO plumes around 700 hPa is captured in MOZAIC and MOPITT data and GEOS-Chem simulation (Figures 4, 5, 6), while in the upper troposphere, the elevated CO is missed in MOZAIC data but captured by GEOS-Chem (Figure 11), and weakly detected by MOPITT (Figure 6b). Because both MOPITT and MOZAIC data only show the sum of CO from all sources so we used fire data and GEOS-Chem simulation to separate different sources. We have replaced the word "confirm" with "recognized" to express ourselves more clearly (L458). We have made the sections more balanced with the observations and simulations. We have commented on the skill of

both models in Sect. 5.4 (L736-754) and availability and quality of MOPITT data in Sect.5.5 (L757-803).

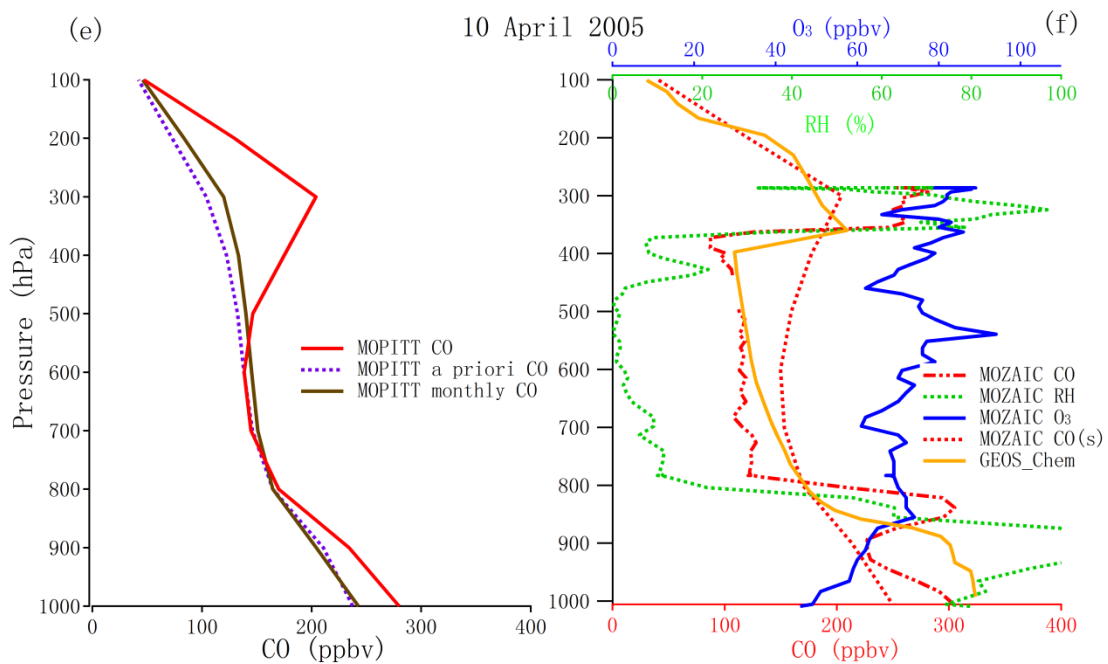
Figure 12 is necessary because it illustrates an important finding in this study (see Sect. 4.2).

p28038, l 1-3 How was this somewhat random time frame chosen? I'm sure there was a good reason, but it's not clear from the text what it was.

Thanks for pointing this out. We did backward trajectories first from the boxed area in Figure 4b, and these trajectories indicate the most particles mainly came from the large fire regions starting from 11 March 2004. We have explained this now in the text (L510-511).

p28038, l 21. It's a bit difficult to believe that different altitude of this plume as identified by MOPITT is an indication of MOPITT's ability to resolve vertical structure. While this could be true given how good MOPITT instrument is in general, the earlier section relied more on GEOS-Chem than MOPITT to even identify the plume, so here I am wondering if we should take MOPITT at face value or wonder what GEOS-Chem is showing in this case.

As mentioned earlier, we did not particularly rely on one dataset or simulation. Instead, we put all the data and simulations together to examine if they support or complement each other. We did examine the GEOS-Chem profile over the boxed area in Figure 4c. GEOS-Chem also shows elevated CO plumes around 400-200 hPa (shown below), which supports the MOZAIC and MOPITT observations. The GEOS-Chem profile was not included in Figure 5f in order to keep it simple and focused, while the signal of the CO plume was illustrated and discussed in Figures 14 and 15.



Section 5 Discussion. It's hard to tell what is the exciting findings. Is it that there was high CO documented? Is it that topography affects vertical CO transport? Is either new and/or surprising? Please tell the reader so. It all seems intuitive and the section is purely qualitative, so it's not clear that anything new is being reported. It would also be helpful to have quantitative information. For example, how does topography affect CO transport, does it have to be a mountain region? only in the north/east/west/south? does any of this or could any of this vary with seasons? It's hard to draw conclusions from individual case studies.

Thanks for the points. The background information is provided in Sect. 5.1 (L650-688). The topography effects are discussed in Sect. 4.2 (L492-496). This section is rewritten to address the reviewer questions. The main contributions of this study include (1) observing rare high CO episodes in the free troposphere in East Asia, (2) identifying distinct transport mechanisms, pathways, and CO sources for these episodes, (3) supporting and extending a proposed mechanism of the leeside troughs over the Indochina peninsula in promoting vertical transport of pollutants, and (4) analyzing MOPITT data from perspective of its vertical sensitivity at synoptic scale (L633-803).

p28044, l28-29 It's not clear why the statistical analysis couldn't be done here already. Authors should consider doing at least preliminary work on that.

In the previous manuscript, we suggested this work as a direction for further studies. This suggested work requires long-term analysis, or at least longer than 5 year. In order to provide accurate statistics, careful examinations of each WCB for the period are needed. This is a large undertaking itself and also beyond the scope of this study. It does not affect the conclusions of this study.

p28045-28046. These whole pages (and the remainder of that section) can be deleted, especially the first paragraph. It's just repeating background information.

This part is largely shortened. The application of MOPITT data is one of the major focuses of this study so some discussion on this perspective is desirable. We now emphasize more on new insights gained from this study (L755-803).

p28048, l17 replace "interplaying" with "interacting"?

Replaced (L840).

Figures: figure captions and labels are a bit too small to be readable, especially on figures 1-7, figure 11.

Figure captions and labels are enlarged for these figures.

Uplifting of carbon monoxide from biomass burning and anthropogenic sources to the free troposphere in East Asia

K. Ding^{1,6}, J. Liu^{1,2,6,*}, A. Ding^{1,6}, Q. Liu^{1,6}, T. L. Zhao³, J. Shi⁴, Y. Han¹, H. Wang⁵, F. Jiang⁵

¹School of Atmospheric Sciences, Nanjing University, Nanjing, Jiangsu, 210093, China

²University of Toronto, Toronto, Ontario, M5S 3G3, Canada

³Nanjing University of Information Science & Technology, Nanjing, Jiangsu, 210044, China

⁴Institute of Remote Sensing Applications, Chinese Academy of Sciences, Beijing, 100101, China

⁵International Institute for Earth System Sciences, Nanjing University, Nanjing, Jiangsu, 210093, China

⁶Collaborative Innovation Center of Climate Change, Jiangsu, 210093, China

To: Atmospheric Chemistry and Physics

| January 2015

*Corresponding author

Abstract

East Asia has experienced rapid development with increasing CO emission in the past decades. Therefore, uplifting CO from the boundary layer to the free troposphere in East Asia can have great implications on regional air quality around the world. It can also influence global climate due to the longer lifetime of CO at higher altitudes. In this study, three cases of high CO episodes in the East Asia China Sea and the Sea of Japan from 2003 to 2005 are examined with spaceborne Measurements Of Pollution In The Troposphere (MOPITT) data, in combination with aircraft measurements from the Measurement of Ozone and Water Vapor by Airbus In-Service Aircraft (MOZAIC) program. High CO abundances of 300-550 ppbv were observed in MOZAIC data in the free troposphere during these episodes. These are among the highest CO abundances documented at these altitudes likely occurring 2-4% in time in the respective altitudes over the region. Correspondingly, elevated CO was shown in MOPITT daytime data in the middle to upper troposphere in the 2003 case, mostly in the lower to middle troposphere in the 2004 case, and in the upper troposphere in the 2005 case. Through analyses of the simulations from a chemical transport model GEOS-Chem and a trajectory dispersion model FLEXPART, we found different CO signatures in the elevated CO and distinct transport pathways and mechanisms for these cases. In the 2003 case, CO from large forest fires near Lake ~~-~~Baikal dominated the elevated CO, which had been rapidly transported upward by a frontal system from the fire plumes. In the 2004 case, anthropogenic CO from the North China Plain experienced frontal lifting and mostly reached ~700 hPa near the East China Sea, while CO from biomass burning from

24 | Indochina experienced orographic lifting, leeside-trough induced convection, and frontal
25 | lifting through two separate transport pathways, leading to two distinct CO enhancements
26 | around 700 hPa and 300 hPa. In the 2005 case, high CO of ~300 ppbv, observed in the
27 | MOZAIC data around 350 hPa, originated from the anthropogenic source over the
28 | vicinity of the Sichuan basin and biomass burning from Indochina, after convection and
29 | strong frontal lifting. These cases show that topography affects vertical transport of CO in
30 | East Asia via different ways, including orographic uplifting over the Hengduan
31 | Mountains, assisting frontal lifting in the North China Plain, and facilitating convection
32 | in the Sichuan basin. In particular, topography-induced leeside troughs over Indochina
33 | lead to strong convection that assisted CO uplifting to the upper troposphere. This study
34 | shows that the new daytime MOPITT near-infrared (NIR) and thermal-infrared (TIR)
35 | data (version 5 or above) have enhanced vertical sensitivity [in the free troposphere](#) and
36 | may help qualitative diagnosis of vertical transport processes in East Asia.

37

38 | **1 Introduction**

39 | Carbon monoxide (CO) plays several important roles in the atmosphere. The
40 | oxidizing capability, an ability of the atmosphere to cleanse itself, is strongly influenced
41 | by the CO level in the troposphere. CO near the surface is a major pollutant, ~~harmful to~~
42 | ~~human health.~~ Under high NO_x conditions, CO is a precursor of ozone, while in low NO_x
43 | airmasses, CO helps ozone destruction (Jacob, 1999; Holloway et al., 2000). As carbon
44 | dioxide (CO₂) is produced in both ozone production and destruction processes (Holloway
45 | et al., 2000), CO is linked to the global carbon cycle (Suntharalingam et al., 2004;
46 | Yurganov et al., 2008; Nassar et al., 2010) affecting climate change. With a lifetime of

47 weeks to months, CO is a good tracer tracking transport of pollution. In the purview of
48 these roles, it is important to understand processes influencing the CO distribution and
49 variability in the atmosphere.

50 Although the main sources of atmospheric CO and its mean status are generally
51 understood (Novelli et al., 1998; Jacob, 1999; Holloway et al., 2000), many processes
52 influencing CO variations at different time scales are not well known. Uplifting CO from
53 the boundary layer to the free troposphere (FT) is such a process, which usually occurs on
54 the synoptic scale that spans hundreds to thousands of kilometers in space and lasts hours
55 to days in time (Daley, 1991). Uplifted CO usually has a longer lifetime and can be
56 transported fast by the upper layer winds over long distances through continents and
57 between hemispheres in the troposphere (Stohl, 2001; Stohl et al., 2002; Damoah et al.,
58 2004). Uplifting air mass from the surface to FT generally takes place by three processes
59 (1) frontal lifting, (2) orographic lifting, and (3) deep convection (Brown et al., 1984;
60 Banic et al., 1986; Dickerson et al., 1987; Bethan et al., 1998; Pickering et al., 1998;
61 Chung et al., 1999; Donnell et al., 2001; Kowol-Santen et al., 2001; Cooper et al., 2002;
62 Liu et al., 2003; Miyazaki et al., 2003; Chan et al., 2004; Mari et al., 2004; Li et al., 2005;
63 Liu et al., 2006; Kar et al., 2008; Zhao et al., 2008; Ding et al., 2009; Randel et al., 2010;
64 Chen et al., 2012).

65 East Asia has experienced rapid development with increasing CO emission in the
66 past decades (Duncan et al., 2007). In addition to impacts on local air quality (Wang et al.,
67 2010), continuing increase in CO emissions will lead to great impacts on regional air
68 quality (Jaffe et al., 1999; Bertschi et al., 2004) and climate (Berntsen et al., 1999) of the
69 world because of an expected upward trend in pollution outflow from the region. East

70 Asia is characterized by its unique and complex meteorology, topography, and land
71 covers. Vertical transport of CO can be modulated by one or more of these conditions or
72 by their interactions. For example, the likelihood of when and where extratropical
73 cyclones are active is closely linked to the locations and frequency of frontal uplifting.

74 ~~Two regions are identified by Chen et al. (1991): one in the East China Sea and the Sea of~~
75 ~~Japan, the other over the leeside of the Altai-Sayan.~~ Wet and dry convections prevail in
76 different seasons in northern China because of the distinct climatological pattern in
77 precipitation there (Dickerson et al., 2007). The topography there also plays an important
78 role in uplifting of CO alone and/or interplaying with frontal systems, aiding convection
79 in mountainous regions (Liu et al., 2003; Ding et al. 2009). Recently, Lin et al. (2009)
80 proposed a new mechanism that emphasizes the impact of topography-induced leeside
81 troughs over Indochina on strong convection. A variety of land cover types in East Asia
82 make CO sources there diversified. In highly populated urban areas, such as those in the
83 North China Plain, anthropogenic emissions are high. Large biomass burning, occurring
84 in areas with abundant vegetation, can generate great amounts of CO for vertical
85 transport when meteorological conditions become favorable. Two such areas are
86 Southeast Asia and the boreal forested area in Russia (Wotawa et al., 2001; Schultz, 2002;
87 Duncan et al., 2003). So far, our understanding of the impacts of these processes and their
88 interactions on CO uplifting is still rather limited (Dickerson et al., 2007). The objectives
89 of studying vertical transport of CO in East Asia are to better understand the vertical
90 distribution of CO in the region, to advance the assessment of impacts of long-range
91 transport of Asian CO on regions downwind, and to help improve simulating this process
92 in atmospheric models on the synoptic scale, eventually leading to more realistic

93 chemical weather forecast in the future (Lawrence et al., 2003).

94 ~~—~~Due to lack of continuous measurements, most studies on CO in East Asia are
95 based on observations from periodic field campaigns (Jacob et al., 2003; Tsutsumi et al.,
96 2003; Li et al., 2007; Ding et al., 2009) or simulations by chemical transport models
97 (Berntsen et al., 1999; Bey et al., 2001) or both (Liu et al., 2003). CO measurements from
98 satellites provide unprecedented data revealing CO variations over East Asia. One of the
99 instruments is the Measurements Of Pollution In The Troposphere (MOPITT)
100 (Drummond, 1992; Drummond and Mond, 1996), ~~which is onboard of the Terra-~~
101 ~~satellite.~~ MOPITT provides data of CO total column and CO vertical profiles at several
102 altitude levels, which are retrieved using a nonlinear optimal estimation method
103 theoretically based on the observed radiances and their weighting functions, the a priori
104 information, and the retrieval averaging kernels (Rogers, 2000; Deeter et al., 2003). As a
105 result, the MOPITT retrieval at one level can be ~~contaminated~~influenced by CO at other
106 levels and thus MOPITT vertical resolution is coarse, generally having only 2-3 pieces of
107 independent information vertically in the troposphere. MOPITT's vertical sensitivity
108 ~~becomes a concern~~was an issue in earlier applications of MOPITT data (Jacob et al.,
109 2003). Nevertheless, a few studies (Deeter et al., 2004; Kar et al., 2004, 2006, 2008; Liu
110 et al., 2006) demonstrated MOPITT's vertical sensitivity to some extent. Kar et al. (2004)
111 found Asian summer monsoon plumes in MOPITT CO data as a strong enhancement of
112 CO in the upper troposphere over India and southern China. Deeter et al. (2004)
113 illustrated similar distributions of the rain rate and the ratio of MOPITT CO at 350 hPa to
114 at 850 hPa in the Tropical Eastern Pacific Ocean. Liu et al. (2006) observed large
115 differences (20-40 ppbv) in MOPITT CO at 250 hPa between two cases of vertical

116 | transport of CO and attributed the differences to the respective weather systems.

117 | Furthermore, the MOPITT data in new versions that use both thermal infrared and near
118 | infrared radiances have offered enhanced vertical sensitivity (Worden et al., 2010; Deeter
119 | et al., 2012; 2013). Therefore, a detailed examination of MOPITT's vertical sensitivity in
120 | East Asia, especially for its ability in detecting vertical transport of high CO episodes, is
121 | desirable.

122 | In this study, three cases of high CO episodes in East Asia from 2003 to 2005 are
123 | examined with MOPITT satellite data, in combination with aircraft measurements from
124 | the Measurement of Ozone and Water Vapor by Airbus In-Service Aircraft (MOZAIC)
125 | program (Marenco et al.,1998) (see Sects.2 and 4). The vertical transport mechanisms
126 | are analyzed with simulations from a trajectory dispersion model FLEXPART (Stohl et
127 | al., 2005) and a chemical transport model GEOS-Chem (Bey et al.,2001), along with
128 | other meteorology data and satellite fire data (see Sects.2 and 4).~~The~~ MOPITT data are
129 | analyzed in two ways. First, the vertical sensitivity of MOPITT is ~~first~~ evaluated with the
130 | coincident ~~MOPITT and~~ MOZAIC data ~~from 2003 to 2005~~ (see Sect.3) and further
131 | illustrated ~~throughout the analysis of with~~ the three high CO episodes in comparison with
132 | the MOZAIC data (see Sect.4). Second, the vertical variation in CO captured by
133 | MOPITT is used to diagnose vertical transport of CO (see Sect. 4). Discussion on the
134 | three cases is synthesized in Sect.5 and the major conclusions are provided in Sect.6.

136 | **2 Model and data**

137 | **2.1 Satellite MOPITT CO data**

138 | MOPITT is the first space instrument that targets continuous measurements of

139 tropospheric CO. MOPITT has been onboard of the Terra satellite launched in 1999,
140 making scientific measurements since March 2000. Terra is flying in a sun synchronous
141 polar orbit with an altitude of 705 km, crossing the equator at ~10:45 and 22:45 LT and
142 making 14-15 daytime and nighttime overpasses each day. MOPITT uses a
143 cross-track scanning method with a swath of 29 pixels, (4 pixels in a row), each of
144 the pixel being ~~22km x 22km~~ 22 km × 22 km. Therefore, with a swath of ~600 km, only
145 about one third of the global area is covered in a day. Additionally, clouds can cause even
146 more gaps in MOPITT daily data. This makes it challenging to use MOPITT data for
147 synoptic studies. It takes 3 days to achieve a near-complete global coverage and 16 days
148 for a complete global coverage (Edwards et al., 1999) if assuming no blocks from clouds.

149 MOPITT measures upwelling radiation in two narrow infrared spectral regions for
150 CO retrieval: (1) a thermal-infrared (TIR) band near 4.7 μm that has strong carbon
151 monoxide absorption and (2) a near-infrared (NIR) band near 2.3 μm that has weak CO
152 absorption. MOPITT Version 5 retrieval products are significantly different from earlier
153 products and offer three distinct products depending on application requirements.

154 One of them is a TIR/NIR “multispectral” product, which has enhanced sensitivity to CO
155 in the lower-most troposphere (Worden et al., 2010; Deeter et al., 2012); 2013).

156 Validations and evaluations of MOPITT data in various versions are documented in
157 Emmons et al. (2004), Worden et al. (2010), and Deeter et al. (2012, 2013).

158 We first examined the MOPITT vertical sensitivity through comparison between
159 coincident MOPITT and MOZAIC CO profiles. Advances of Version 5 (V5, a TIR/NIR
160 “multispectral” product) from Version 4 (V4, a TIR-only product) data were assessed with the level 2 data. Then, V5 level 2 data were used throughout the case studies, in

162 | which MOPITT data were gridded horizontally into 0.25 °latitude ~~xx~~ 0.25 °longitude and
 163 | at the MOPITT vertical resolution of 100 hPa from the surface to 100 hPa.

164 |

165 | 2.2 Aircraft MOZAIC CO data

166 |

167 | The Measurement of Ozone and Water Vapor by Airbus In-Service Aircraft
 168 | (MOZAIC) program was initiated in 1993 by European scientists, aircraft manufacturers,
 169 | and airlines to collect experimental data (Marenco et al., 1998). MOZAIC consists of
 170 | automatic and regular measurements of ozone, CO, and water vapor by several
 171 | long range passenger airliners flying all over the world. The aim is to build a large
 172 | database of measurements to allow studies of chemical and physical processes in the
 173 | atmosphere.

174 | In comparing MOPITT with MOZAIC CO data, coincident MOPITT and MOZAIC
 175 | data from 2003 to 2005 were screened within a radius of 1.5 °and within a ~~4h period.~~
 176 | Each 4 h period. The radius of 1.5 °was applied to selected MOZAIC profiles at 500 hPa
 177 | and the MOZAIC slant path was included in the radius. MOZAIC profile was smoothed
 178 | by applying the MOPITT averaging kernels and the a priori profile for the co-located
 179 | retrieved MOPITT profile to account for the bias introduced by the averaging kernels and
 180 | the a priori. Therefore, the smoothed MOZAIC CO profile $\hat{\mathbf{x}}^{MOZAIC}$ is derived by
 181 | (Rogers, 2000)

$$182 | \hat{\mathbf{x}}^{MOZAIC} = \mathbf{x}_a^{MOPITT} + \mathbf{A} (\mathbf{x}^{MOZAIC} - \mathbf{x}_a^{MOPITT}) \quad (1)$$

183 | where ~~a=xx~~ $\mathbf{A} = \partial \hat{\mathbf{x}} / \partial \mathbf{x}$ is the MOPITT averaging kernel matrix which describes the
 184 | sensitivity of the MOPITT CO estimate to the true profile of CO, \mathbf{x}^{MOZAIC} is the

185 MOZAIC CO
186 _profile, which has been mapped to the MOPITT pressure grid. The quantity x_a^{MOPITT} is
187 the MOPITT a priori, which is based on CO simulations from the MOZART model
188 (Emmons et al., 2004).

189 The MOZAIC measurements usually extend from the surface to ~~~250hPa~~ 250
190 hPa.

191 When validating MOPITT data using Eq.(1), CO mixing ratios above 300 hPa
192 _was supplemented with CO from the GEOS-Chem chemical transport model
193 (see Sect.2.6) on the same location and day, similar to the treatments by ~~Emmons et~~
194 ~~al.(2004) and~~ Worden et al.(2010), who used the MOZART climatology simulations.

195 Because CO above 250 hPa is lower than that in the middle and lower troposphere, the
196 bias due to this treatment is expected to be low.

197

198 ~~2.3 NCEP FNL meteorological data~~

199 ~~The Final (FNL) global tropospheric analyses are on 1° by 1° grids every 6h~~
200 ~~(<http://rda.ucar.edu/datasets/ds083.2/>). The data are generated from the Global Data~~
201 ~~Assimilation System (GDAS), which continuously collects observational data from the~~
202 ~~Global Telecommunications System (GTS) and other sources. The analyses are available~~
203 ~~on the surface, at 26 levels from 1000 hPa to 10 hPa, the tropopause, the boundary layer,~~
204 ~~two subsurface levels, and a few others. Parameters include surface pressure, sea level~~
205 ~~pressure, geopotential height, temperature, sea surface temperature, potential temperature,~~
206 ~~relative humidity, precipitable water, u and v winds, and vertical motion.~~

208

~~2.4 The~~

2.3 MODIS fire count data

The Moderate-resolution Imaging Spectroradiometer (MODIS) is a type of instruments which have been onboard of the Terra (EOS AM) satellite since 1999 and on the Aqua (EOS PM) satellite since 2002. The MODIS fire products include a validated daily global active fire product (MOD14 Terra and MYD14 Aqua) (Justice et al., 2002), generated using a global active fire detection algorithm that uses a multispectral contextual approach to exploit the strong emission of midinfrared radiation from fires allowing subpixel fire detection (Giglio et al., 2003). The horizontal resolution is 1 km. The fire data are acquired from the Fire Information for Resource Management System (FIRMS) (Davies et al., 2009).

2.4 NCEP FNL meteorological data

The NCEP Final (FNL) global tropospheric analyses are on 1° by 1° grids every 6h (<http://rda.ucar.edu/datasets/ds083.2/>). Parameters in FNL include surface pressure, sea level pressure, geopotential height, temperature, sea surface temperature, potential temperature, relative humidity, precipitable water, u and v winds, and vertical motion, available on the surface, at 26 levels from 1000 to 10 hPa, the tropopause, the boundary layer, and a few others. In addition to driving FLEXPART (see Sect. 2.5), the FNL data are used to analyze the meteorological conditions including the surface pressure, wind fields, and development of a cyclone. The data are generated from the Global Data Assimilation System (GDAS).

233 **2.5 The FLEXPART trajectory model**

234 To diagnose the transport processes and trace CO sources, we used the FLEXPART
235 model (Stohl et al., 2005), which is a Lagrangian Particle Dispersion Model developed at
236 the Norwegian Institute for Air Research in the Department of Atmospheric and Climate
237 Research. FLEXPART can be driven by meteorological input data generated from a
238 variety of global and regional models. In this study, the simulations were driven by the
239 NCEP FNL data. This model has been extensively validated (Stohl et al., 1998;
240 Cristofanelli et al., 2003) and widely used in studies of the influence of various
241 meteorological processes on pollution transport (Cooper et al., 2004, 2005, 2006;
242 Hocking et al., 2007; Ding et al., 2009; Barret et al., 2011; He et al., 2011; Chen et al.,
243 2012). In running FLEXPART, a large number of particles are released from defined
244 locations (latitude, longitude, and altitude) at a time. Backward or forward trajectories of
245 the particles are recorded in latitude (°), longitude (°), and altitude (km) every hour.

247 **2.6 The GEOS-Chem chemical transport model**

248 GEOS-Chem is a global three dimensional chemical transport model
249 (<http://geos-chem.org>). The model contains detailed description of tropospheric
250 O₃-NO_x-hydrocarbon chemistry, including the radiative and heterogeneous effects of
251 aerosols. It is driven by assimilated meteorological observations from the National
252 Aeronautics and Space Administration (NASA) Goddard Earth Observing System
253 (GEOS) from the Global Modeling and Assimilation Office (GMAO). In this study,
254 | GEOS-Chem version v9-1-3 was employed and executed in the full chemistry mode,
255 | which is driven by GEOS meteorology with temporal resolution of 6h (3h for surface

256 meteorological variables), with a horizontal resolution of 2 °latitude by 2.5 °longitude
257 and 47 vertical levels, including ~35 levels in the troposphere from 1000 to ~~100hPa~~100
258 hPa.
259 —_GEOS-Chem uses anthropogenic emissions from the Emissions Database
260 for Global Atmospheric Research (EDGAR) global inventory (Olivier and Berdowski,
261 2001), which are updated with regional inventories, including the emission inventory in
262 Asia (Streets et al., 2006; Zhang et al., 2009). The biomass burning emissions are from
263 the Global Fire Emissions Data (GFEDv3) monthly inventories (van der Werf et al., 2010)
264 and biogenic VOC emissions are taken from the Model of Emissions of Gases and
265 Aerosols from Nature (MEGAN) global inventory. Emissions from other natural sources
266 (e.g., lightning, volcanoes) are also included.

267 The model has been extensively evaluated and used in studies of atmospheric
268 chemistry and pollution transport (Bey et al., 2001; Heald et al., 2003; Liu et al., 2003;
269 Liu et al., 2006; Zhang et al., 2006; Jones et al., 2009; Nassar et al., 2009; Kopacz et al.,
270 2010; Jiang et al., 2011). GEOS-Chem can generally describe CO variability in the
271 troposphere but somewhat underestimate the observations in the northern mid-latitudes
272 possibly due to biases in the CO inventory or numerical diffusion in the model or both
273 (Heald et al., 2003; Duncan et al., 2007; Nassar et al., 2009; Kopacz et al., 2010).

274

275 **3 Comparison between MOPITT and MOZAIC CO profiles**

276 MOPITT's vertical sensitivity can be described in terms of the averaging kernels
277 (see Eq.1) and the Degree of Freedom for Signal (DFS). The averaging kernel matrix
278 indicates the sensitivity of the MOPITT CO estimate to the true CO profile, with I

279 (identity matrix) being the best, when true CO profiles are retrieved, and 0 being the
280 worst, when MOPITT retrievals just take the a priori. In reality, the average kernel matrix
281 is less than I, implying some contaminations contribution of CO from other levels to the
282 retrieved level so that the CO vertical structure cannot be fully resolved. DFS gives the
283 number of independent pieces of information available vertically in the measurements
284 and it is the sum of the diagonal elements of the averaging kernel matrix (Rogers, 2000).

285 Figure 1

286 shows a yearly mean of DFS for daytime and nighttime, respectively, in East Asia
287 for the V5 TIR/NIR data, indicating substantial increases in DFS compared to earlier
288 MOPITT versions (Worden et al., 2010; Deeter et al., 2012). The daytime DFS in East
289 Asia (Fig.1a) ranges from 0.5 to 2.7, usually decreasing with latitude, similar to its
290 distribution in other regions and on the global scale (Deeter et al., 2004; Worden et al.,
291 2010). In the same latitudinal zones, the DFS is higher over land than over ocean. The
292 daytime annual DFS is high in the Sichuan basin, the eastern part of mainland China, the
293 Indochina peninsula, and the Indian subcontinent. Over the mountain or valley regions,
294 DFS is low, such as above the Tibetan Plateau. The stars indicate the cities where
295 MOZAIC vertical measurements are available for validation of MOPITT data. The
296 annual mean DFS is 1.65, 1.51, 1.60, and 1.64, respectively, in an area of $1^\circ \times 1^\circ$ around
297 Beijing, Narita, Shanghai, and Hong Kong, with a maximum of 1.98, 1.64, 1.81, and
298 1.74 for the cities, respectively. The nighttime DFS values (Fig. 1b) are lower (from 0.5
299 to 1.5) than the daytime values, similar to that in Deeter et al. (2004) for an earlier
300 MOPITT version. Spatially, nighttime DFS is high over regions where the daytime DFS
301 is also high.

302 The general patterns of MOPITT averaging kernels have been documented (Pan et
303 al., 1998; [Edwards et al., 1999](#); Emmons et al., 2004; Deeter et al., 2003, 2004, 2012; Kar
304 et al., 2008; Worden et al., 2010). For V5 MOPITT data, the averaging kernels at the four
305 cities are similar to these in Worden et al. (2010, in their Fig. 7). The difference in the
306 averaging kernels between V4 and V5 can be as large as 0.14 [f_{0.14}in](#) the surface and lower
307 troposphere and as 0.10 [f_{0.10}in](#) the upper troposphere (not shown).

308 Figure 2 shows the relative bias between MOPITT and the smoothed MOZAIC
309 (\hat{x}^{MOZAIC}) profiles (see Eq. 1), which is also referred as “MOPITT estimate of in situ” in
310 Worden et al. (2010) and “transferred profile” in Emmons et al. (2004). For V5 data (in
311 red), the mean bias is within $\pm 20\%$ for all the cities. In all the altitude levels, the bias
312 is smallest (close to zero) around 500-400 hPa and increases upward and
313 downward. The bias is mostly positive above 500-400 hPa, while below 500-400 hPa, it
314 is positive at Beijing, Narita but negative at Shanghai and Hong Kong. Whether the sign
315 change is related to the change in the geographic location (Shanghai and Hong Kong are
316 both coast cities) can be a subject for further study. The V4 data (in green) also show the
317 smallest bias in the middle troposphere. In the lower troposphere, the bias in V5 is
318 reduced by 5-10% at Beijing and Narita. At Shanghai and Hong Kong, the bias changes
319 from positive in V4 to negative in V5, with a smaller (at Shanghai) or larger (at Hong
320 Kong) magnitude. In the upper troposphere above 500-400 hPa, the bias in V5 at Beijing,
321 Narita, and Shanghai changes to positive, with a magnitude as the same as or larger than
322 in that in V4. At Hong Kong, the bias in V5 remains positive but the magnitude is
323 enlarged. – [Deeter et al. \(2013\) compared MOPITT data with the NOAA aircraft](#)
324 [measurements over North America and data from the HIAPER Pole to Pole Observations](#)

325 (HIPPO) field campaign data (Wofsy et al., 2011). They found a positive bias in
326 MOPITT V5 TIR/NIR data at 400 hPa (4%) and 200 hPa (14%). They also showed a
327 latitude-dependent positive bias in the northern hemispherical upper troposphere in
328 MOPITT V3 and V4 data. This study suggests an overall positive bias, agreeing with
329 Deeter et al. (2013) in magnitude and sign, in MOPITT V5 data for the upper troposphere.

330 As a comparison, we also validated MOPITT data in other cities in the globe and found
331 that the mean bias in Europe or the United States is lower than in East Asia, especially in
332 the surface layer (not shown).

333 The correlation between MOPITT and smoothed MOZAIC data is shown in Fig. ~~3~~ for
334 the middle to upper troposphere (Fig. 3a) and for the surface to the middle troposphere
335 (Fig. 3b). 3. From 500 to 100 hPa, the correlation coefficient between the two data sets is
336 0.92, 0.86, 0.83, 0.68 at Beijing, Narita, Shanghai, and Hong Kong, respectively (Fig.3a),
337 while from the surface to 600 hPa, the correlation becomes closer, being 0.90,0.92,
338 0.92, 0.94 at Beijing, Narita, Shanghai, and Hong Kong, respectively (Fig. 3b). The
339 correlation coefficient between the two data is the best in the middle troposphere
340 (500-400 hPa, not shown).

341

342 **4 Uplifting of CO to the free troposphere**

343 Daily MOPITT and MOZAIC data from 2003-2005 were screened to find cases of
344 high CO episodes observed by both MOPITT and MOZAIC at the same location and
345 time. We found three cases of high CO in MOPITT data with close-by MOZAIC
346 measurements, while it was hard to find such high CO episodes with exact coincident
347 MOPITT and MOZAIC observations because of large gaps in MOPITT data and limited

348 aircraft sampling coverages. In the three cases, high CO concentrations up to 300-500
349 ppbv are observed by MOZAIC in the free troposphere from 750 to 350 hPa.
350 ~~aircraft sampling coverages.~~ In the following, we provide detailed analyses of each case,
351 ordered by year of occurrence in Table 1. The cases occurred over the East China Sea or
352 the Sea of Japan or both. High CO was shown in MOPITT daytime data in the middle to
353 upper troposphere in case 2003, mostly in the lower to middle troposphere in case 2004,
354 and in the upper troposphere in case 2005. For comparison, MOPITT and MOZAIC
355 observations for the three cases are shown in Figs. 4-6, followed by analyses for each
356 case with FLEXPART and GEOS-Chem simulations, in combination with MODIS fire
357 data and NCEP FNL meteorological data. Table 1 provides a brief summary for all the
358 cases. The cases occurred in spring and summer when cyclone activities are strong in
359 East Asia (Chen et al., 1991; Yue and Wang, 2008). ~~High CO concentrations up to~~
360 ~~300-500 ppbv are observed in FT from 750 hPa up to 350 hPa.~~ The CO sources are
361 identified as biomass burning or a combination of biomass burning and anthropogenic
362 origins. The outflow of the high CO episodes finally reached the boundary layer at the
363 west coast of the United States and Canada.

364

365 **4.1 Case study I: 6 June 2003**

366 On 6 June 2003, a large area (~ 400 km ~~x~~ 1500 km) of high CO up to 350 ppbv
367 appeared in the MOPITT image over the Sea of Japan and the nearby continent in the
368 middle to high troposphere (Fig. 4a). ~~The area with high CO is the largest among the~~
369 ~~three cases, reflecting the strongest CO source from large forest fires in this case.~~
370 In Fig. 5a, the MOPITT CO profile averaged over the boxed area in Fig. 4a shows a

371 | broad enhancement from the monthly profile between ~~800~~650-300 hPa, with peak CO
372 | abundances of ~300 ppbv appearing around 550 hPa. The large difference between the
373 | MOPITT a priori and the measurements over these altitudes indicates MOPITT's
374 | ~~capability of capturing pollution episodes with some degree of vertical sensitivity.~~
375 | capability of capturing pollution episodes with some degree of vertical sensitivity. The
376 | vertical sensitivity is demonstrated through (1) the strongest CO source among the three
377 | cases was captured by the largest magnitude of CO enhancement of 200-250 ppbv from
378 | the a priori, (2) the altitude of the maximum CO enhancement was detected around the
379 | middle troposphere, in contrast to the other two cases which show the maximum in the
380 | lower-middle and upper troposphere, respectively, and (3) the elevated CO was over a
381 | broad range of altitudes as the vertical resolution of MOPITT is rather coarse, i.e., the
382 | maximum DFS is about 2.5 (Figure 1). This CO peak was not shown in the MOPITT
383 | monthly mean profile, reflecting the episodic nature of this event. The high CO episode
384 | was also captured by a near-by MOZAIC
385 | measurement (Fig. 5b). A layer of elevated CO is apparent between 500-350 hPa, with a
386 | CO peak up to ~ 550 ppbv around 400 hPa. In addition, the MOZAIC relative humidity
387 | (RH) and ozone profiles are shown in Fig. 5b. Around the altitudes of CO buildup,
388 | elevated humidity followed the CO profile, while ozone also showed some enhancement.

389 | A latitude-altitude cross section from MOPITT is shown in Fig. 6a. It is the average
390 | between two blue dashed lines in Fig. 4a. The arrows represent the winds in the
391 | meridional and vertical directions and the contour represents the zonal wind speed.
392 | Consistent with Fig. 4a, high CO up to 350 ppbv appears in the middle to upper
393 | troposphere between 35-~~50N. The CO buildup was with the highest abundance and the~~

394 | ~~widest depth among the three cases, reflecting again the strongest CO source in this~~
395 | ~~case.~~ 50°N.

396 | To trace down the CO source, backward trajectories of the air particles were
397 | simulated using FLEXPART after releasing 30 000 and 7000 particles, respectively, from
398 | the locations of the large and small boxed areas in Fig. 6a (the same as the blue bars in
399 | Fig. 4a) on 6 June 2003 when CO was high in the MOPITT data. Because CO has a
400 | relatively long lifetime (weeks to month), it is assumed that CO is not removed in the
401 | backward trajectories. Figure 7 shows the distribution of particle concentration between
402 | 6.25-10.25 km (~ 500-250 hPa, Fig. 7a) and between 0-3.25 km (~ 1000-650 hPa,
403 | Fig.7b). The contour lines indicate the geopotential height at 850 hPa at 12:00 UTC on 3
404 | June 2003 (Fig. 7a) and at 0 UTC on 2 June 2003 (Fig. 7b), respectively. The stars,
405 | diamonds, and circles in Fig. 7b show the location of large forest fires near Lake Baikal
406 | from MODIS fire data. The circles, diamonds, and stars denote daily mean fire counts of
407 | 20-100, 100-300, and 300-500 per ~~2.5~~ 2.5 × ~~2.5~~ 2.5 ° grid area, respectively, from 31 May to 6
408 | June. The high particle counts between 0-3 km in the vicinity of Lake Baikal match well
409 | with the location of fire counts (Fig. 7b). On 3 June 2003, there was a cyclone with a cold
410 | frontal system (Fig. 7a) that rapidly lifted the CO originated from the fires along the
411 | warm conveyor belt (WCB) to the upper level. The particle distribution in the upper
412 | troposphere shows the transport pathway of the particles to the Sea of Japan. To further
413 | illustrate this, particles were released from the fire region near Lake Baikal (93-115 °E,
414 | ~~50-65~~ 50-60 °N, 0-3 km, following ~~Lavoue~~ Lavoué et al. (2000), who found an average
415 | injection height of Siberian fires of ~ 3 km). Forward trajectories were simulated and the
416 | resultant vertical distribution of the particles varying with time during 1-15 June 2003 is

417 shown in Fig. 8. It is found that the released particles from the fires traveled along the
418 isobars to northeast of Lake Baikal from 1 June to 3 June 2003 and then the particles
419 were lifted to the upper layers (3-8 km) on 3 June at 12 a.m. (in 60-70 h) (Fig. 8). Then,
420 the particles were transported to the east along these altitudes. On 6 June (in 120-140 h),
421 a large amount of particles appeared in a layer of 3-8 km (Figs. 8 and 4a). The altitudes
422 with high particle concentrations agree ~~remarkably~~ well the MOPITT data between
423 ~~500~~650-350 hPa (Figs. 4a and 6a).

424 It is the cyclone with a ~~w~~ front northeast of Lake Baikal that transported the CO up
425 along the WCB (Figs. 7a and 8). Figure 5b shows that the relative humidity reached about
426 65 % in MOZAIC measurement, suggesting the air mass indeed came from a WCB
427 (Cooper et al., 2002). The MOZAIC ozone profile also shows elevated ozone at the same
428 altitudes but the shape does not follow exactly the ones of CO and humidity, implying
429 complexity of chemical processes involved. The polluted air reached as high as 9 km
430 although most particles remained at heights of about 3-8 km (Fig. 8). After being lifted to
431 higher altitudes, the polluted air was transported by strong westerlies over long distances.
432 Figure 8 shows that the particles were further transported to the east and sink slowly after
433 7 June. Around 14 June 2003, the particles reached the east coast of Canada (0-5 km).
434 The satellite MODIS data show a large number of hot spots near Lake Baikal in May and
435 June 2003. Earlier studies have shown that forest fires in Asia can impact air quality in
436 North America (Jaffe et al., 2004; Liang et al., 2004; Oltmans et al., 2010). This case
437 illustrates again the role that WCBs played in the intercontinental transport of pollution
438 for such high CO. It should be noted that the FLEXPART simulation was made by using
439 the FNL meteorological data, which may have not considered the buoyancy force due to

440 fires. Such buoyancy force can lift CO plumes even faster and higher. ~~Our analyses are~~
441 ~~also consistent with Nedelec et al. (2005), who analyzed 320 MOZAIC flight routes from~~
442 Our analyses are consistent with Nédélec et al. (2005), who analyzed 320 MOZAIC
443 flight routes from Europe to Asia in 2003 and reported the observations of high CO up to
444 800 ppbv above 8 km (~ 350 hPa) on 3 and 4 June 2003 around 57 °N (northeast of Lake
445 Baikal). This matches well with the time and location of frontal lifting of CO in this
446 FLEXPART simulation. With analyses of different data sets, i.e., Along Track Scanning
447 Radiometer (ATSR) fire data, the Total Ozone Mapping Spectrometer (TOMS) aerosols
448 data and the MODIS cloud data, ~~Nedelee~~Nédélec et al. (2005) also attribute the high CO
449 at these altitudes to front lifting of CO from large forest fires near Lake Baikal.

450 Furthermore, this analysis provides a detailed description on the CO transport pathways
451 (Figs. 7 and 8). We found that this case, caused by the strongest CO source among the
452 three cases, show the largest horizontal area with CO plumes (Fig. 5), the widest vertical
453 CO buildup with strongest abundances (Fig. 7), and the biggest enhancement of 200-250
454 ppbv from the a priori (Fig. 6).

456 **4.2 Case study II: 18 March 2004**

457 This case occurred on 18 March 2004 when high CO appeared in the MOPITT data
458 in the lower and middle troposphere over the East China Sea (Fig. 4b). The elevated CO
459 of 200-250 ppbv is observed between 750 ~~hPa~~ and 550 hPa vertically in MOPITT data
460 (Fig. 5c). The departure of the MOPITT CO profile from ~~it's~~its a priori reflects the
461 MOPITT's vertical sensitivity (Fig. 5c). The MOPITT monthly mean, like for the other
462 two cases, follows a typical CO profile pattern with CO concentrations being the highest

463 near the surface and decreasing gradually with altitude. The CO on 18 March 2004 was
464 50 ppbv higher than the monthly mean above 800 hPa. A layer of large elevated CO
465 appeared in the MOZAIC profile between 750-550 hPa with a peak of 500 ppbv around
466 650 hPa (Fig. 5d). The high RH (~ 90-100 %) below 600 hPa in the MOZAIC data
467 suggests that the air mass experienced some uplifting process that enhanced its humidity,
468 likely from a WCB. The MOZAIC ozone peaked (~ 70 ppbv) around the same altitudes
469 as CO, implying that ozone may be produced in the air mass carrying high CO during the
470 transport process. Figure 6b shows a latitude-altitude cross section averaged between the
471 two blue dashed lines in Fig. 4b. Around 30°N, elevated CO levels (~ 200 ppbv) are
472 evident around 700 hPa. The corresponding winds (blue lines and arrows) show that there
473 were strong descents north of the elevated CO and moderate ascents in the south of the
474 region (Fig. 6b), indicating the formation of a frontal system with downward and upward
475 flows, south and north of the front, respectively.

476 This case was simulated with GEOS-Chem to identify the sources of CO and to
477 explore the transport mechanisms. The MODIS fire data suggest biomass burning over
478 northern Indochina peninsula to be a source for the observed high CO (Fig. 9). The time
479 series of fire counts over area of 20-25 °N and 92-105 °E peaked on 12 March 2004.
480 Correspondingly, high CO of ~ 300 ppbv appeared in the MOPITT composite of 11-18
481 ~~May~~March 2004 at 700 hPa over northern Indochina peninsula (Fig. 9). ~~This source is~~
482 ~~confirmed in~~In the GEOS-Chem simulation (Fig. 10b-), this source is also recognized. In
483 addition, the anthropogenic source concentrated over the North China Plain (NCP)
484 (approximately 30-40 °N, 110-125 °E) is identified as another source of high CO ~~in the~~
485 ~~GEOS-Chem simulation~~ (Fig. 10c). Figure 11 shows the latitude-altitude cross sections of

486 the GEOS-Chem simulations of CO, fire-induced CO, and anthropogenic CO,
487 respectively, along 130 °E on 18 March 2004. The CO from biomass burning was more
488 widely spread to the south than the anthropogenic CO. CO abundances from both sources
489 were high around 700 hPa (Fig. 11b and c) between 25-35 °N across 130 °E where
490 MOPITT observed high CO (Fig. 6b).

491 The different CO distributions for the two sources in three dimensions (Figs. 10 and
492 11) reflect rather different transport pathways and uplifting mechanisms. The transport of
493 the fire-induced CO can be divided into the following four processes. First, the CO was
494 orographically lifted along the Hengduan Mountains from the surface to ~ 750 hPa. The
495 lifted CO is shown in Fig. 12 around 100 °E on a longitude-altitude cross section
496 along 22 °N. Then, the CO experienced two separate transport pathways. In the second
497 process, part of the lifted CO was further transported upward to 400-300 hPa, shown as a
498 bulb in Fig. 12 around 105 °E. This is due to strong convection, possibly caused by ~~by~~
499 frontal system developed on March 17, 2004 (Fig. 9), interplayed with the leeside troughs
500 east of the Hengduan Mountains. The vertical velocity reached ~~0.2m2 m~~ 0.2 m s^{-1} in FNL data
501 around ~~at~~ this level (not shown). The ECMWF (European Centre for Medium-Range
502 Weather Forecasts) data also show northeastward airflow from Indochina peninsula with
503 high potential energy (warm and wet) available for strong convection. All of these
504 suggest that the strong convection over the leeside troughs rapidly lifted CO up to ~350
505 hPa. In fact, the orographic lifting and topography-induced convection are quite common
506 in this region so high CO often appears at these two altitudinal levels in March as
507 simulated by GEOS-Chem (not shown). On 17 March, the lifted CO was with even
508 higher concentrations ~~were even higher~~ (~ 500 ppbv) around 400 hPa than the monthly

509 mean because of the high CO source from large forest fires. In the third process, the
510 uplifted CO around 400-300 hPa (near 105 °E in Fig. 12) was transported northeastward
511 by strong winds along the front in the upper troposphere, reaching the East China Sea
512 (near 30 °N, 130 °E) on 18 March (Figs. 10b and 11b). This transport enables high CO
513 from forest fires in southern Asia in low latitudes to rapidly reach the upper troposphere
514 in the mid-latitudes. In the fourth process, paralleling to the second and third, part of the
515 orographically lifted CO stayed around ~~~700hPa~~700 hPa because of leeside-trough
516 induced convection. This CO was transported eastward along the isobars of the low
517 pressure system around 700 hPa (Figs. 10 and 12). This process occurred at lower
518 altitudes than processes two and three. The transport was slower and it took longer time
519 (from 15 to 18 March) for the CO to reach the East China Sea. Processes two and three
520 brought CO to the upper troposphere, while process four increased CO in the lower to
521 middle troposphere (Fig. 11b). For the anthropogenic CO in the North China Plain, the
522 vertical transport was mainly carried out by frontal lifting. Horizontally, anthropogenic
523 CO was transported eastward along 30 °N (Fig. 10c). Consequently, the total CO shows a
524 buildup centered near 700 hPa around 30 °N and 130 °E, mostly coming from the two
525 CO sources (Fig. 11a-c).

526 The Hengduan Mountains run mainly north to south, with elevations ranging from
527 1300 to 6000 metres. This topography provides a favorable condition for the formation of
528 the leeside troughs if meteorology is satisfied. Such troughs promote vertical transport of
529 CO on the west flank of the Mountain (in the second and fourth processes), while the
530 orographic lifting occurred on the east flank of the Mountains (in the first process).

531 Comparison of the simulated vertical structure of CO (Fig. 11a) with the MOPITT

532 observation (Fig. 6b) shows that MOPITT can generally capture vertical transport of CO
533 from forest fires and anthropogenic sources, although the magnitude of CO in MOPITT
534 data was lower and there were also substantial gaps in the MOPITT images due to
535 convective clouds. In the MOPITT data, high CO of ~ 200 ppbv reached up to 200 hPa.
536 In the lower to middle troposphere, elevated CO (~ 200 ppbv) was centered around
537 650-700 hPa. These features are similar to the GEOS-Chem simulations. Note that the
538 CO buildup around 300 hPa in the GEOS-Chem simulation (Fig. 11a and b) was reflected
539 in the MOPITT data (Fig. 6b), but not as obvious as in the simulation since the MOPITT
540 retrievals are smoothed with the averaging kernels. This CO is also shown as a little
541 bump around 300 hPa in MOPITT vertical profile in Fig. 5c. This buildup is missing in
542 the MOZAIC profile (Fig. 5d) because the aircraft flew towards the north and outside the
543 region with high CO.

544 In FLEXPARTAs the backward trajectories starting from the boxed area in Figure
545 4b indicated the most particles came from the large fire regions starting from 11 March
546 2004, air particles were released in FLEXPART over the ~~large fire~~ regions from the
547 surface to 1 km on 11 March 2004. ~~FLEXPART was used, and forward trajectories were~~
548 simulated to ~~simulate transport of~~track down the air parcels until 18 May 2004 at 2 a.m.

549 Taking the same zonal means as for Fig. 6b, it is found that the vertical distribution of
550 particle concentrations is similar to that in Fig. 6b with highest particle concentrations
551 between 4-5 km (not show). As simulated by FLEXPART, the outflow of the high CO
552 finally reached the west coast of the United

553 States with particles mainly distributed around 5 km in altitude. High CO observed
554 in East Asia in this case appeared the most southerly among the three, leading to a most

555 southerly outflow.

556 The transport mechanism of biomass burning by the fourth processes was first
557 proposed by Lin et al. (2009) who found ~~a significant role~~ that the leeside troughs above
558 the Indochina peninsula play a significant role in uplifting of ozone ~~from biomass~~
559 ~~burning there~~ as there is lack of tropical deep convection to explain such strong
560 convection. In this study, we even found these leeside troughs promote vertical transport
561 of CO to the upper troposphere (the second process, Fig. 12). It is the interplay of the
562 leeside troughs and the cyclone in the northeast of China which formed a front system
563 that transported CO from the Indochina peninsula upward. _

564

565 **4.3 Case Study III: 10 April 2005**

566 In this case, MOPITT observed high CO of ~ 250 ppbv at 300 hPa near the east coast
567 of Japan on 10 April 2005 (Fig. 4c). To compare MOPITT and MOZAIC data, the mean
568 MOPITT profile was taken over a boxed area (in Fig. 4c) upwind of the MOZAIC
569 measurement. The MOPITT vertical profile clearly shows a CO peak around 300 hPa,
570 where it departs from the MOPITT monthly mean (Fig. 5e). Comparing with cases 2003
571 and 2004, MOPITT CO peaked at higher altitudes, illustrating some MOPITT vertical
572 sensitivity even at these altitudes. In Fig. 5f, a sharp peak of 300 ppbv in MOZAIC CO
573 is shown around 350 hPa. The profile of relative humidity ~~followed~~follows closely that of
574 CO, with
575 values up to 90-100 % around ~~300~~350 hPa, implying that the elevated CO was lifted to
576 this level from the lower troposphere by a cyclone system along its WCB. However, the
577 MOZAIC ozone profile varies ~~strongly~~differently from the CO and relative humidity

578 profiles. This ~~wasis~~ found ~~to be~~ due to a strong stratospheric intrusion introduced by the
579 cyclone. HYSPLIT simulations suggest that a large amount of ~~airmass~~ ~~air mass~~ plunged
580 around 4 ~~June~~ ~~April~~ from 9 to 3-4 km over northwest of China, bringing high ozone to the
581 lower troposphere (not shown). Miyazaki et al. (2003) also observed downwelling of
582 stratospheric air on the
583 ~~back~~ side of cyclones. Figure 6c shows an altitude-latitude cross section averaged
584 between 120-150 °E (between two dashed lines in Fig. 4c). High CO of 200-250 ppbv
585 appeared between 300-200 hPa around 35 °N. This is a rare case in which MOPITT
586 reports such high CO (200-250 ppbv) at these high altitudes (around 300 hPa).
587 Documented CO abundances observed by MOPITT at these altitudes were ~130 ppbv
588 over Indian summer monsoon seasons (Kar et al., 2004), 110-150 ppbv in the North
589 America from the forest fires, chemical, and anthropogenic sources (Liu et al., 2005;
590 ~~2006~~), and ~150 ppbv in spring at Hong Kong (Zhou et al., 2013).

591 The MODIS fire data show that there were indeed large fires over Indochina
592 peninsula in 3-10 April 2005, shown as stars in Fig. 13. Using GEOS-Chem, CO from
593 fire and anthropogenic sources was simulated to identify their respective contributions
594 and transport pathways.

595 The entire process of vertical transport of CO is well reproduced by GEOS-Chem
596 (Fig. 14). Figure 14a provides the CO distribution in the lower troposphere on 8 April
597 2005, while ~~FigFigs~~. 14b and ~~e14c~~ show the CO distribution on the next day and the day
598 after in the middle and upper troposphere, respectively. The geopotential heights at 750,
599 450, and 250 hPa are overlaid with the CO ~~image~~ ~~images~~ for each layer accordingly. On 8
600 April 2005, there was a cyclone developing in the east of Lake Baikal between 110-120 °

601 E, 45-55 °N. The surface CO was transported upward and northeastward along the WCB
602 (Fig. 14a). On 9 April, the cyclone moved to the east (Figs. 13 and 14b). The high CO
603 shows a “comma” shape along WCB at the mid-troposphere; this shape is typical for a
604 mature cyclone system with a WCB (Cooper et al., 2002). The cyclone further moved
605 eastward and reached the Sea of Japan on 10 April (Fig. 14c). The GEOS-Chem
606 simulation shows accumulation of high CO over the ridge of high pressure and along the
607 front at the
608 upper troposphere. The GEOS-Chem simulations suggest that the outflow of the
609 high CO reached Canada on 16 April.

610 The combined effects of cyclone activities, topography, and CO from different
611 sources and locations are reflected in distinct CO signatures along the WCB. Figure 15
612 shows the CO from the fires (FigFigs. 15a and e15c) and from the anthropogenic source
613 (FigFigs. 15b and d15d) in the middle and upper troposphere, respectively, overlaid with
614 the geopotential height at 450 hPa (FigFigs. 15a and b15b) and 250 hPa (FigFigs. 15c and
615 d15d), respectively. In the middle troposphere (500-400 hPa), a large amount of CO from
616 the fires in Indochina peninsula was uplifted to this level along the middle part of the
617 WCB on 9 April 2005 and was transported eastward on 10 April, 2005 (Fig. 15a). One
618 source of the anthropogenic CO was concentrated around the North China Plain (Ding et
619 al., 2009) where high CO was evident in MOPITT data (Fig. 13, 35-45 °N, 100-120 °E)
620 (Fig. 15b). On 8 April, this CO was uplifted along the WCB and further transported to the
621 middle troposphere, coming across sudden elevated terrains on the way and forming the
622 head of the “comma” in the cyclone system (Figs. 14b and 15b). The topography's role
623 was noticed by Liu et al. (2003), who found a ring of convergence around the North

624 China Plain associated with elevated terrain, and by Ding et al. (2009), who speculated
625 possible topography lifting in North China Plain. In the southern end of the WCB (near
626 30 °N, 120 °E in Fig. 15b), the CO came from the anthropogenic source in the vicinity of
627 the Sichuan basin (~ 26-34 °N, 102-110 °E). This CO was transported vertically to 500
628 hPa on 8 April at 18:00 UTC to 9 April at 00:00 UTC. Air pollution often accumulates in
629 the Sichuan basin because of its special topography. The development of small scale
630 cyclones there is well known as the southwest vortex or Sichuan low (Tao and Ding,
631 1981). Accumulated pollutants there usually are transported to the free troposphere by
632 such convection. The strong convection can last more than 6 h and peak at the midnight
633 (Yu et al., 2007). As this anthropogenic source is quite stable, its contribution should not
634 be understated.

635 Interestingly, Lin et al. (2009) reported an observed ozone enhancement from
636 ozonesonde data at 4 km in Taiwan on 11 April 2005. They proposed a new transport
637 mechanism from their study as discussed in Sect. 4.2, in which they attributed the
638 elevated ozone to the biomass burning in Indochina. Similarly, CO from biomass burning
639 is also apparent over Taiwan at the ~~midtroposphere~~middle troposphere in the
640 GEOS-Chem simulation (Fig. 15a), although the maximum CO enhancement was north
641 of Taiwan at this altitude.

642 The white dot in Fig. 15 indicates the location where MOZAIC passed over. It is clear
643 that MOZAIC measurement was within the WCB at 200-300 hPa, while it was at a
644 distance from the WCB at 500-400 hPa. This is consistent with the MOZAIC CO profiles
645 shown in Fig. 5f, suggesting that MOZAIC in fact measured air from the stratosphere at
646 these altitudes. As the wind was stronger in the upper than in the lower troposphere, the

647 WCB-transported CO reached further east in the upper levels (Fig. 15). The simulations
648 suggest that over the boxed area in the MOPITT image in Fig. 4c at 300 hPa, the fire and
649 anthropogenic sources each contributed about ~ 20 % of the observed CO. Comparing
650 the GEOS-Chem simulation (Fig. 14c) with the MOPITT observation (Fig. 4c), we
651 noticed that there were large gaps in MOPITT data north of 35 °N where CO abundances
652 were
653 even higher than the MOPITT measurements south of 35 °N. These gaps were caused
654 by clouds associated with the cyclone system. The complication due to clouds is a
655 problem
656 with an optical instrument like MOPITT, which explains why it is hard to find cases like
657 this in which high CO can be observed by both MOPITT and MOZAIC under a frontal
658 condition.

659 In this case, the strong part of the front (close to the centre of the cyclones) swept
660 southern China, where CO was high (Fig. 13). Along the front (30-40 °N, 100-120 °E),
661 the temperature gradient at 925 hPa was as high as 4.9 C per degree. Strong ascents
662 occurred ahead of the front, with vertical velocity being ~0.05 m s⁻¹ at 900 hPa and ~
663 0.220 m s⁻¹ at 750 hPa, and increasing with altitude until 300-250 hPa where the
664 maximum vertical velocity was 0.25926 m s⁻¹. Consequently, the high CO can be rapidly
665 lifted to the upper troposphere in this case.

666 FLEXPART was also used to trace down high CO in the MOPITT image by releasing
667 air particles in the boxed area in Fig. 6c (indicated by a bar in Fig. 4c). We found that the
668 most CO came from the southwest part of China (boxed area in Fig. 13) where MOPITT
669 CO composite of 3-10 April 2005 shows high CO of 250-300 ppbv. This CO was lifted

670 along the WCB described above. This agrees with the GEOS-Chem simulation which
671 shows the major contribution of the anthropogenic source to CO in the upper troposphere,
672 likely from the Sichuan Basin (Fig. 15d).

673

674 **5 Discussion**

675

676 New insights gained from this study and suggestions for future work are discussed as
677 follows.

678 **5.1 Observations of high CO episodes**

679 In the three CO episodes, high CO abundances ~~above 300-550~~ ppbv were observed
680 ~~in aircraft by~~ MOZAIC ~~data~~ in the free troposphere ~~over East Asia during 2003-2005. In~~
681 ~~cases 2003 and 2004, the peak value reached 500 ppbv. In case 2005, CO concentration~~
682 ~~of 300 ppbv was observed at the upper troposphere (~300 hPa). These are (Fig 5). The~~
683 elevated CO abundances are among the highest ~~CO abundances which have been~~
684 documented at these altitudes in East Asia. Ding et al. (2009) observed high CO episode
685 of ~1185 ppbv at 2.6 km (850-700 hPa) over the North China Plain in summer 2007.
686 ~~NedeleeN et al.~~ et al. (2005) found CO up to 800 ppbv above 8 km (~400 hPa) near the
687 fire region of Lake Baikal on 3 and 4 June 2003. Highest CO concentrations during
688 TRACE-P were between 250-300 ppbv from 2-12 km (Heald et al., 2003; Liu et al., 2003;
689 Miyazaki et al., 2003). Occurrences of such high CO episodes are not by chance. They
690 reflect the uniqueness and complexity of meteorology, orography, vegetation covers, and
691 CO sources in East Asia. For example, in all the cases, biomass burning occurred from
692 regions with dense vegetation covers and with most active forest fires in East Asia

693 (Schultz, 2002; Duncan et al., 2003). These fires are usually most active in summer in
694 boreal forest in Russia, like in case 2003, and in spring in the southern East Asia, like
695 cases 2004 and 2005, enhancing chances of high CO episodes in these seasons.

696 The ~~possibility~~frequency of occurrences of such high CO is ~~further~~ illustrated in
697 Table 2. As the three cases ~~occurred~~occurred near Japan, MOZAIC data around the
698 vicinity of Narita ~~and its surrounding areas~~ from 2001 to 2006 are summarized, showing
699 occurrences of various CO abundance ranges in the boundary layer (the surface-850 hPa),
700 the lower (850-600 hPa), middle (600-400 hPa), and upper (400-200 hPa) troposphere.
701 Among all the data in the upper troposphere, CO abundances occurred 93 times (17-%)
702 between 200-300 ppbv, 19 times (4-%) between 300-400 ppbv, and 6 times (1%) over
703 400 ppbv. In the middle troposphere, the fraction of occurrences of CO within 200-300,
704 300-400, and over 400 ppbv was ~~14-%, 3-%, and 2-%~~, respectively. In the boundary layer,
705 the highest occurrences of CO abundances (38-% of all the data in the layer) were within
706 200-300 ppbv, while the range was within
707 100-200 ppbv in the lower (47-%), middle (74-%), and upper troposphere (66-%).
708 Seasonally, there were more high CO occurrences in the higher altitudes in spring and
709 summer than in fall and winter.

710 ~~This study illustrates that the topography in East Asia can affect vertical transport of CO~~
711 ~~in different ways.~~ The frequency of such high CO episodes is also examined in the
712 GEOS-Chem simulations and MOPITT observations in the vicinity of Narita (126-140 °E
713 30-40 °N) in 2005 (Table 3). For the GEOS-Chem simulations, a count is added to a CO
714 range if the daily maximum CO in the area at a layer falling into that CO range. Thus, the
715 total counts for all the CO ranges at a given layer are 365, while the counts are 281 for

716 MOPITT due to missing data. To minimize noise in daily MOPITT data, only when there
717 were at least 10 data with the maximum CO values falling into a given CO range, a count
718 is added. GEOS-Chem can simulate CO up to 400 ppbv in the upper troposphere, while
719 the maximum CO in MOPITT data is lower so that different CO ranges are used in Table
720 3. Overall, MOZAIC, MOPITT and GEOS-Chem all show a high frequency of high CO
721 (larger than 200 ppbv) at the surface, gradually shifting to a high frequency of low CO
722 (less than 200 ppbv) at the upper troposphere. Between 400-200 hPa, CO episodes with
723 200-300 ppbv occurred 1.2 times every 10 days in GEOS-Chem, slightly lower than in
724 MOPITT (1.8 times) and MOZAIC (1.7 times). Overall, MOZAIC observes 2-5% more
725 transport of high CO to the upper troposphere than GEOS-Chem, while the latter
726 simulates 10-20% more transport of CO (with lower abundances) to the middle and lower
727 troposphere.

728 It is likely that on average, the extremely high CO episodes like the three cases (Fig.
729 5) occurred 2-4 times per 100 days in their respective altitudes over the East China Sea
730 and the Sea of Japan (Tables 2 and 3). As stated, air mass with lower CO abundances of
731 200-300 ppbv can be transported to 400-200 hPa in a frequency of 1-2 times per 10 days
732 (Tables 2 and 3). The frequency can be even higher in spring and summer (Table 2),
733 approximately once a week. Significant impacts of such transport can be expected on the
734 air quality downwind and on the global climate. The transport mechanisms and CO
735 source contributions revealed in this study can also be applicable for these CO episodes,
736 even with lower CO abundances or at lower altitudes.

737

738 5.2 The role of topography

739 East Asia's topography varies significantly across its vast width, increasing from east
740 to west, with a variety of terrains. This study found that topography there affected the
741 three cases in different ways. In addition to its general function in orographic lifting (in
742 case 2004), topography ~~can~~ also interplay with frontal systems and enhance the uplifting
743 substantially in the North China Plain (in cases 2004 and 2005). Under the influence of
744 the Tibetan Plateau, the southwest vortex (or the Sichuan low) is formed (Tao and Ding,
745 1981) and can facilitate strong convection in the Sichuan basin (in case 2005).

746 In particular, topography-induced convection due to the leeside troughs east of the
747 Hengduan Mountains, ~~first~~ proposed by Lin et al. (2009), offers a new mechanism for
748 vertical transport of pollutions from the region (in case 2004). Lin et al. (2009) mainly
749 aimed at vertical transport of pollutions to the lower and middle troposphere. Extending
750 from Lin et al. (2009), this study found it possible to explain pollution transport to the
751 upper troposphere using such a mechanism.

752

753 5.3 The implications of WCB trends on uplifting of CO

754 Extratropical cyclones and associated frontal activities are important in lifting CO
755 from the boundary layer to the free troposphere. ~~This can be harmful to regions~~
756 ~~downwind because the lifted CO can be transported for a long distance by strong upper~~
757 ~~level winds (Stohl et al., 2001, 2002; Damoah et al., 2004).~~ This also applies to other
758 air pollution. Zhao et al. (2008) found that the influence of Asian dust storms on North
759 American ambient particulate matter levels is highly related to the height to which the
760 frontal cyclones in East Asia can lift dust. Although the functions and characteristics of
761 WCBs have been recognized by earlier studies, this study provides some details unique

762 for the three cases. In case 2004, we found that it is the interplay of the leeside troughs
763 and the cyclone in the northeast of China which formed a front system that transported
764 CO from the Indochina peninsula upward. This case also appeared the most southerly
765 among the three, leading to a most southerly outflow. In case 2005, we found
766 downwelling of stratospheric clean air on the back side of cyclones. We also found that
767 anthropogenic CO from two regions and CO from biomass burning dominated different
768 parts of a WCB. The source allocation was sensitive to the location of the front.
769 Comparing cases 2004 and 2005, we found that when large CO source coincided with the
770 strongest part of a WCB, uplifting of CO to the upper troposphere became more possible.
771 ~~the frontal cyclones in In East Asia can lift dust. This study shows that when air masses~~
772 ~~with high CO coincide with the strongest part of a WCB, uplifting of CO to the upper~~
773 ~~troposphere is possible. East Asia is one of two regions between 25–45 °N with most~~
774 ~~frequent WCB events (Eckhardt et al., 2004). Inside East Asia, there are two regions~~
775 ~~where, cyclones occur most frequently in two regions in spring and summer: one over the~~
776 ~~lee sides of the Altai-Sayan and the other in the East China Sea and the Sea of Japan,~~
777 ~~occurring mostly in spring and summer over both regions (Chen et al., 1991; Yue and~~
778 ~~Wang, 2008). The seasons and locations of~~
779 ~~three cases just match well with these two areas and active cyclone seasons, which should~~
780 ~~not be taken by chance.~~ These are the locations and seasons where and when we can
781 expect similar events to happen in the future. Chen et al. (1991) suggested a decline in
782 cyclonic events in East Asia from 1957 to 1977 and no such decline from 1977 to 1987.
783 Recently, an analysis for a longer term from 1951 to 2010 based on ensembles of
784 Twentieth Century Reanalysis (20CR) showed a decreasing trend in the northern part of

785 the Sea of Japan and an increasing trend over the southern part of the Sea of Japan and
786 the leeside of the Altai-Sayan in summer (Wang et al., 2013). The implications of these
787 trends on uplifting of CO deserve further ~~studying.~~

788 ~~Biomass burning is identified as an important source for all three episodes,~~
789 ~~suggesting that CO from sporadic fire activities can provide an additional source to the~~
790 ~~less-varying anthropogenic emissions and enhance chances of high CO episodes. The fire~~
791 ~~regions shown in this study are the places with dense vegetation covers and with most~~
792 ~~active forest fires in East Asia (Schultz, 2002; Duncan et al., 2003). These fires are~~
793 ~~usually most active in summer in boreal forest in Russia, like in case 2003, and in spring~~
794 ~~in the southern East Asia, like cases 2004 and 2005.~~

795 ~~–GEOS-Chem and FLEXPART simulations reveal different CO signatures from~~
796 ~~biomass burning and anthropogenic sources in the high CO episodes, reflecting different~~
797 ~~transport pathways and mechanisms and locations of both sources. In case 2003, CO from~~
798 ~~large forest fires near Lake Baikal dominated the elevated CO, which had been~~
799 ~~rapidly transported upward by a frontal system from the fire plumes. In case 2004,~~
800 ~~anthropogenic CO from the North China Plain experienced frontal lifting and mostly~~
801 ~~reached ~700 hPa near the East China Sea, while CO from biomass burning experienced~~
802 ~~orographic lifting, leeside troughs induced convection, and frontal lifting through two~~
803 ~~separate transport pathways, leading to two distinct CO enhancements around 700 hPa~~
804 ~~and 300 hPa. In case 2005, along a WCB in the East China Sea and the Sea of Japan,~~
805 ~~anthropogenic CO from the North China Plain and from the Sichuan basin prevailed in~~
806 ~~the northern and southern part of the WCB, while CO from biomass burning in Indochina~~
807 ~~and southern China was mostly distributed in the middle. The source allocation is very~~

808 sensitive to the location of the front. Overall, the anthropogenic sources contributed more
809 than biomass burning to the CO in the middle and upper troposphere in this
810 case investigation. It would be helpful to conduct statistical analysis of the CO source
811 distribution along WCBs in East Asia in the future.

812

813 5.4 Comparison between observations from aircraft and satellite and 814 model simulations

815 Pollution transport can be tracked computationally with Euler and Lagrangian
816 approaches, as represented by GEOS-Chem and FLEXPART models, respectively.
817 GEOS-Chem can not only track transport of CO (a physical process) but also consider
818 chemical reactions during the transport while FLEXPART can visualize transport
819 pathways and pin down source regions effectively, without considering chemical
820 functions in the meantime. GEOS-Chem can also fill the gaps in MOPITT~~MOPITT~~
821 satellite data ~~eam~~ (Figs. 10, 11, and 14). This study found that GEOS-Chem simulated the
822 observed aircraft and satellite CO well in cases 2004 and 2005 but cannot fully reproduce
823 the elevated CO in MOZAIC data in case 2003. The CO plume is simulated in lower
824 mixing ratios at lower altitudes than in the MOZAIC data. The plume also appeared
825 further ~~extend MOZAIC CO observations north.~~ This is possibly due to an
826 underestimated fire inventory or conservative parameterizations in simulating large forest
827 fires or both in GEOS-Chem. Nassar et al. (2009) reported underestimates of CO by
828 GEOS-Chem over the 2006 Indonesia fire region, in comparison with the Tropospheric
829 Emission Spectrometer (TES) observations. FLEXPART can generally simulate the three
830 cases, strikingly well sometimes in agreement with observed details in space and time.

831 although discrepancies between FLEXPART and satellite and aircraft observations can
832 be found in various places on small scales.~~larger areas and over wider altitude ranges.~~
833 ~~High CO concentrations were observed by MOPITT over thousand kilometers~~
834 ~~horizontally and a few kilometers vertically~~ FLEXPART is good at simulating strong
835 sources, while weak sources sometimes are omitted.

836

837 5.5 Applications of MOPITT data

838 We analyzed MOPITT data from two aspects: vertical sensitivity on the synoptic
839 scale. ~~Such variations of CO~~Both are ~~usually diluted~~challenging and have not been
840 studied adequately.

841 Large gaps due to clouds and the limited MOPITT swath make application of
842 MOPITT on longer time scales. ~~Earlier application~~the synoptic scale difficult. Thus
843 application of MOPITT ~~CO~~ data over East Asia were mostly focused on monthly or
844 seasonal ~~CO variations~~scales (Tanimoto et al., 2008; Zhao et al., 2010; Hao et al., 2011;
845 Liu et al., 2011; Zhou et al., 2013; Su et al., 2014). ~~The~~This study shows that even with
846 large gaps, daily MOPITT data can capture vertical disturbances of CO on the synoptic
847 scale, which are usually diluted on longer time scales. This study also suggests the
848 importance of filling the gaps with other satellite data or in designing new ~~understanding~~
849 ~~of synoptic disturbances from MOPITT and MOZAIC data in this study can help improve~~
850 ~~simulation of synoptic processes in atmospheric models, eventually leading to more~~
851 ~~realistic chemical weather forecast in the future (Lawrence et al., 2003)~~satellite
852 instruments, for the purpose of detecting such variation over large area on the regional
853 and global scales.

854 ~~MOPITT CO retrievals were validated with the MOZAIC aircraft observations at~~
855 ~~four cities in East Asia after taking the MOPITT averaging kernels and the a priori into~~
856 ~~consideration. In the upper troposphere, MOPITT V5 retrievals are usually higher than~~
857 ~~the MOZAIC measurements, while in the lower troposphere, MOPITT retrievals are~~
858 ~~higher than MOZAIC measurements in Beijing and Narita but lower at Shanghai and~~
859 ~~Hong Kong. The mean relative biases in all~~Typically for satellite remote sensing products,
860 the MOPITT retrieval at a specific pressure level is influenced by CO from other levels
861 are within 20 %,
862 with the lowest and thus its retrieval at that pressure level can be bias around 500–400 hPa
863 (close to zero). The DFS of MOPITT V5 is generally enhanced compared with the V4
864 product.

865 ~~While MOPITT provides unprecedented new datasets for.~~ However, MOPITT can
866 more accurately measure average CO mixing ratio over a better understanding of the
867 atmospheric chemistry, thick layer. This results in a coarse vertical resolution and the
868 vertical variation in CO seemed not to be fully resolved in earlier applications of
869 MOPITT data (Jacob et al., 2003). ~~Nevertheless, some studies suggest that~~ This study
870 addressed the MOPITT indeed has some vertical sensitivity. ~~with newly Kar et al.~~
871 ~~(2004) found Asian summer monsoon plumes in MOPITT COV5 data as a strong~~
872 enhancement of CO and found enhanced vertical sensitivity in V5 data in the free
873 troposphere, even the upper troposphere over India and southern China., in addition to in
874 the boundary layer emphasized by Worden et al. (2010) and Deeter et al. (2004)2012).
875 The enhanced DFSs and the averaging kernels in V5 illustrated similar
876 distributions of the rain rate and the ratio of MOPITT CO at 350 to at 850 hPa in the

877 ~~Tropical Eastern Pacific Ocean. Liuby Worden et al. (2006) observed large differences~~
878 ~~(20-40 ppbv) in MOPITT CO at 250 hPa between two cases of vertical transport of CO~~
879 ~~and attributed the differences to the respective weather systems. In this study, MOPITT's~~
880 ~~vertical sensitivity with the new V5 retrievals is well illustrated in three cases with high~~
881 ~~CO episodes (Figs. 5 and 6). In Fig., (2010) and Deeter et al. (2012) are supported (Fig.~~
882 ~~3 and Sect.3).~~

883 In Fig. 5, the smoothed MOZAIC profiles were calculated using the averaging
884 kernels and the a priori in an area upwind of the MOZAIC measurement within 0-5 °
885 distance for each case as there were no MOPITT data available at the locations of the
886 MOZAIC measurements. Although this may introduce some bias, the smooth averaging
887 kernel smoothed MOZAIC profiles in V5 show more vertical structure in CO than an
888 earlier version of MOPITT data in Jacob et al. (2003). ~~Because the CO retrieval at a~~
889 ~~certain pressure level is often contaminated by CO from other levels, in other words, the~~
890 ~~averaging kernel matrix is less than I, MOPITT cannot specify the exact height of~~
891 ~~elevated CO shown in the MOZAIC measurement. The magnitude of elevated CO in~~
892 ~~MOPITT retrievals was much lower than in the MOZAIC data at altitudes where CO~~
893 ~~peaked and thus the vertical variation of CO was still much smoothed in MOPITT data.~~
894 ~~However, spatial variation in MOPITT CO data can show elevated CO in the lower,~~
895 ~~middle, and upper troposphere in the respective cases. The strong CO source in case 2003~~
896 ~~is reflected differently from the other two cases. The vertical distribution of CO over~~
897 ~~large area and in a wide range of altitudes shown in Fig. 6 for the three cases matches~~
898 ~~with simulations of GEOS-Chem and FLEXPART, sometimes remarkably well. (2003).~~
899 The detection of high CO in the upper troposphere in case 2005 makes MOPITT data

900 promising in studying vertical transport of CO or the vertical distribution of CO
901 qualitatively up to that level. Overall, this study found: (1) MOPITT can differentiate the
902 magnitude of different CO plumes (Figs. 5 and 6), (2) MOPITT can distinguish elevated
903 CO in the lower, middle, and upper troposphere (Figs. 5 and 6), (3) the shape of CO
904 plumes in vertical direction matches with simulations of GEOS-Chem and FLEXPART,
905 sometimes remarkably well (Fig.6), and (4) there is more vertical structure in CO in new
906 V5 than in earlier versions of MOPITT data (Fig. 5).

907 It is the relative variations in MOPITT CO data that help diagnose of CO transport
908 vertically or horizontally. This study suggests using MOPITT data quantitatively with
909 caution, especially at altitudes with high CO plumes, as illustrated that the magnitude of
910 elevated CO in MOPITT retrievals can be lower than in the MOZAIC data at altitudes
911 where CO peaked (Fig. 5). Therefore, the vertical variation of CO, even enhanced in V5,
912 is still much smoothed in MOPITT data. MOPITT can distinguish elevated CO in
913 different layers of the free troposphere, yet sometimes cannot specify the exact altitude of
914 elevated CO shown in the MOZAIC measurements (Fig. 5). One limitation for MOPITT's
915 application of vertical transport is the complication of clouds, which often accompany
916 frontal systems. As shown in cases 2004 and 2005, CO is usually high in cloudy areas.

917 Therefore, the magnitude of CO abundances can be ~~statistically~~-underestimated by
918 MOPITT in these areas. ~~Large gaps due to clouds and the limited MOPITT swath make it~~
919 ~~challenging to use MOPITT data for studying synoptic processes.~~

920 ~~Pollution transport can be tracked computationally with Euler and Lagrangian~~
921 ~~approaches, as represented by GEOS-Chem and FLEXPART models, respectively. The~~
922 ~~two models have successfully reproduced the observed aircraft and satellite CO to some~~

~~extent. GEOS-Chem can not only track transport of CO (a physical process) but also consider chemical reactions during the transport while FLEXPART can visualize transport pathways and pin down source regions effectively, without considering chemical functions in the meantime. GEOS-Chem can also fill the gaps in MOPITT satellite data (Figs. 10, 11, 14). GEOS-Chem simulates cases 2004 and 2005 well but cannot reproduce the magnitude of the elevated CO in MOZAIC data in case 2003, possibly because its parameterization of large forest fires was conservative or the fire emissions were underestimated in the inventory. Nassar et al. (2009) reported underestimates of CO by GEOS-Chem over the 2006 Indonesia fire region, in comparison with the Tropospheric Emission Spectrometer (TES) observations. FLEXPART can generally simulate the three cases, strikingly well sometimes in agreement with observed details in space and time, although discrepancies between FLEXPART and satellite and aircraft observations can be found in various places on small scales.~~

6 Conclusions

East Asia is characterized by its unique and complex meteorology, topography, vegetation covers, and CO sources. The characteristics are reflected in uplifting of CO illustrated in three high CO episodes during 2003-2005 in this study. Through integrated analyses of observations from the airborne MOZAIC ~~aircraft~~ and ~~thespaceborne~~ MOPITT ~~satelliteinstruments~~ and simulations from a trajectory dispersion model FLEXPART (Stohl et al., 2005) and a chemical transport model GEOS-Chem (Bey et al.,

946 | 2001), this study draws the ~~major~~following conclusions.

947 | ~~conclusions as follows.~~

948 | 1.—In the three CO episodes, high CO abundances of 300-550 ppbv are observed in

949 | aircraft MOZAIC data in the free troposphere- over the East China Sea and the Sea

950 | of Japan. These are among the highest CO abundances ever documented at these

951 | altitudes. The three cases occurred in the

952 | 1. seasons and at locations where meteorological and CO source conditions are

953 | favorable for such episodes. It is likely that on average, such high episodes occur

954 | 2-4 times per 100 days at the respective altitudes in the region. CO episodes in

955 | lower altitudes and with lower abundance occur more frequently in the region,

956 | about 1-4 times every 10 days with 200-300 ppbv in 600-400 hPa.

957 | 2.—GEOS-Chem and FLEXPART simulations reveal different CO signatures from

958 | biomass burning and anthropogenic sources in the CO enhancement in the three

959 | cases, reflecting different transport pathways and mechanisms and locations of both

960 | sources. In case 2003, CO from large forest fires near Lake Baikal dominated the

961 | elevated CO. In case 2004, anthropogenic CO came from the North China Plain

962 | and mostly reached ~ 700 hPa near the East China Sea, while CO from biomass

963 | burning ~~from~~in Indochina was transported through two separate pathways, leading

964 | to two distinct CO enhancements around 700 hPa and 300 hPa. In case 2005, along

965 | 2. a WCB over the East China Sea and the Sea of Japan, anthropogenic CO from

966 | the North China Plain and from the Sichuan basin prevailed in the northern and

967 | southern part of the WCB, while CO from biomass burning in Indochina ~~and~~

968 | ~~southern China~~ was mostly distributed in the middle part of the WCB.

969 | ~~3.~~ Topography in East Asia influences vertical transport of CO in different ways. In
970 | particular, topography-induced leeside troughs east of the Hengduan Mountains
971 | over Indochina lead to strong convection. This new mechanism proposed by Lin et
972 | al. (2009) is ~~confirmed~~supported by this study in explaining CO transport to the
973 | middle troposphere and further extended ~~in this study for CO transport to the upper~~
974 | troposphere. Strong convection
975 | 3. from the Sichuan basin also plays an important role in vertically transporting
976 | anthropogenic CO ~~to the free troposphere.~~ The topography ~~interplaying~~interacting
977 | with frontal ~~activates~~activities can enhance the vertical transport of CO
978 | substantially in North China Plain.

979 | 4. Extratropical cyclones and associated frontal activities are important mechanism in
980 | lifting CO from the boundary layer to the free troposphere, as illustrated by the
981 | three cases and ~~many~~ earlier studies. East Asia is one of two regions between 25-45 °
982 | N with most frequent WCB events (Eckhardt et al., 2004). Inside East Asia, there
983 | are two regions where cyclones occur most frequently: one over the lee sides of the
984 | Altai-Sayan and the other in the East China Sea and the Sea of Japan, occurring
985 | mostly in spring and summer over both regions (Chen et al., 1991). The seasons
986 | and locations of the three high CO episodes just match well with these two areas
987 | and active cyclone seasons, which may not happen by chance.

988 | 5. Biomass burning is identified as an important source for all three episodes,
989 | suggesting that CO from sporadic fire activities can provide additional CO to less
990 | varying anthropogenic emission and enhance chances of high CO episodes. The
991 | fire regions shown in this study are the places with dense vegetation covers and

992 with most active forest fires in East Asia.

993 6. The MOPITT's vertical sensitivity is found to be enhanced in its new V5 NIR/TIR
994 data- in the free troposphere, even in the upper troposphere. The daytime V5 data
995 can detect synoptic ~~disturbance~~disturbances of weather systems on horizontal
996 variation of CO. The data also show more vertical structure than earlier versions
997 and can distinguish CO enhancements at different layers of the troposphere,
998 although the detected high CO is over a broad range in altitudes and lacks detailed
999 vertical structure in comparison with the aircraft observations. Because the CO
1000 retrieval at a ~~~~~certain pressure level is often ~~contaminated~~smoothed by CO from
1001 other levels, the MOPITT retrievals usually underestimate elevated CO peaks
1002 ~~during the~~at altitudes with high CO ~~episodes~~plumes. The complication of clouds
1003 within frontal systems can generate large gaps in MOPITT data and cause
1004 underestimation of CO statistically in these regions. Nevertheless, MOPITT data
1005 may be used to qualitatively help diagnose vertical transport processes, with
1006 caution on their absolute CO values. ~~In general, MOPITT substantially~~
1007 ~~underestimates CO in high CO episodes and, on~~On average, MOPITT slightly
1008 ~~overestimates~~overestimates the background CO in the upper troposphere.

1010 **Acknowledgements.**

1011 The authors gratefully acknowledge the following data and modeling tools. The
1012 satellite CO data are provided by the MOPITT team and acquired from the NASA
1013 Langley Research Center Atmospheric Science Data Center. The MOZAIC CO data are
1014 from the European Commission, Airbus, and the Airlines (Lufthansa, Austrian, Air

1015 France) who carry free of charge the MOZAIC equipment and perform the maintenance
1016 since 1994. The Final Analysis Data (FNL) were obtained from NOAA CDC. The
1017 GEOE-Chem model is developed and managed by the Atmospheric Chemistry Modeling
1018 Group at Harvard University with support from the NASA Atmospheric Chemistry
1019 Modeling and Analysis Program (ACMAP). The FLEXPART model development team
1020 consists of Andreas Stohl, Sabine Eckhardt, Harald Sodemann, and John Burkhardt at the
1021 Norwegian Institute for Air Research (NILU). [Insights and critiques from two](#)
1022 [anonymous reviewers are highly appreciated.](#) Financial support is provided by an open
1023 fund from the Institute of Remote Sensing and Digital Earth, Chinese Academy of
1024 Sciences (OFSLRSS201107), the Key Basic Research Program (2010CB950704,
1025 2014CB441203), and the Natural Science Foundation of China (41375140).

1026

1027 **References**

1028

1029 Banic, C. M., Isaac, G. A., Cho, H. R., and Iribane, J. V.: The distribution of pollutants
1030 near a frontal surface: a comparison between field experiment and modeling, *Water Air*
1031 *Soil Poll.*, 30, 171-177, 1986.

1032

1033 Barret, B., Le Flochmoen, E., Sauvage, B., Pavelin, E., Matricardi, M., and Cammas, J. P.:
1034 The detection of post-monsoon tropospheric ozone variability over south Asia using IASI
1035 data, *Atmos. Chem. Phys.*, 11, 9533-9548, doi:10.5194/acp-11-9533-2011, 2011.

1036

1037 Berntsen, T. K., Karlsdóttir, S., and Jaffe, D. A.: Influence of Asian emissions on the
1038 composition of air reaching the north western United States, *Geophys. Res. Lett.*, 26,
1039 2171-2174, doi:10.1029/1999GL900477, 1999.

1040

1041 Bertschi, I. B., Jaffe, D. A., Jaeglé L., Price, H. U., and Dennison, J. B.: PHOBEA/ITCT
1042 2002 airborne observations of trans-Pacific transport of ozone, CO, VOCs and aerosols to
1043 the northeast Pacific: impacts of Asian anthropogenic and Siberian Boreal fire emissions,
1044 *J. Geophys. Res.*, 109, D23S12, doi:10.1029/2003JD004328, 2004.

1045

1046 Bethan, S., Vaughan, G., Gerbig, C., Volz-Thoms, A., Richer, H., and Tiddeman, D. A.:
1047 Chemical air mass differences near fronts, *J. Geophys. Res.*, 103, 13413-13434, 1998.

1048

1049 Bey, I., Jacob, D. J., Yantosca, R. M., Logan, J. A., Field, B. D., Fiore, A. M., Li, Q., Liu,
1050 H. Y., Mickley, L. J., and Schultz, M. G.: Global modeling of tropospheric chemistry with
1051 assimilated meteorology: model description and evaluation, *J. Geophys. Res.*, 106,
1052 23073-23095, 2001.

1053

1054 Brown, R. M., Daum, P. H., Schwartz, S. E., and Hjelmfelt, M. R.: Variations in the
1055 chemical composition of clouds during frontal passage, in: *The Meteorology of Acid
1056 Deposition*, edited by: Samson, P. J., Air Pollut. Control Assoc., Pittsburgh, Pa., 202-212,
1057 1984.

1058

1059 Chan, D., Yuen, C. W., Higuchi, K., Shashkov, A., Liu, J., Chen, J., and Worthy, D.: On
1060 the CO₂ exchange between the atmosphere and the biosphere: the role of synoptic and
1061 mesoscale processes, *Tellus B*, 56, 194-212, 2004.

1062

1063 Chen, B., Xu, X. D., Yang, S., and Zhao, T. L.: Climatological perspectives of air
1064 transport from atmospheric boundary layer to tropopause layer over Asian monsoon
1065 regions during boreal summer inferred from Lagrangian approach, *Atmos. Chem. Phys.*,
1066 12, 5827-5839, doi:10.5194/acp-12-5827-2012, 2012.

1067

1068 Chen, S., Kuo, Y., Zhong, P., and Bai, Q.: Synoptic climatology of cyclogenesis over East
1069 Asia, 1958-1987, *Mon. Weather Rev.*, 119, 1407-1418, 1991.

1070

1071 Chung, K. K., Chan, J. C. L., Ng, C. N., Lam, K. S., and Wang, T.: Synoptic conditions
1072 associated with high carbon monoxide episodes at coastal station in Hong Kong, *Atmos.
1073 Environ.*, 33, 3099-3095, 1999.

1074

1075 Cooper, O. R., Moody, J. L., Parrish, D. D., Trainer, M., Ryerson, T. B., Holloway, J. S.,
1076 Hübler, G., Fehsenfeld, F. C., and Evans, M. J.: Trace gas composition of midlatitude
1077 cyclones over the western North Atlantic Ocean: a conceptual model, *J. Geophys. Res.*,
1078 107, D7, doi:10.1029/2001JD000901, 2002.

1079

1080 Cooper, O. R., Forster, C., Parrish, D., Dunlea, E., Habler, G., Fehsenfeld, F., Holloway,
1081 J., Oltmans, S., Johnson, B., Wimmers, A., and Horowitz, L.: On the life-cycle of a
1082 stratospheric intrusion and its dispersion into polluted warm conveyor belts, *J. Geophys.
1083 Res.*, 109, D23S09, doi:10.1029/2003JD004006, 2004.

1084

1085 Cooper, O. R., Stohl, A., Hubler, G., Hsie, E. Y., Parrish, D. D., Tuck, A. F., Kiladis, G.
1086 N., Oltmans, S. J., Johnson, B. J., Shapiro, M., Moody, J. L., and Lefohn, A. S.: Direct
1087 transport of midlatitude stratospheric ozone into the lower troposphere and marine
1088 boundary layer of the tropical Pacific Ocean, *J. Geophys. Res.*, 110, D23310, doi:
1089 10.1029/2005JD005783, 2005.

1090

1091 Cooper, O. R., Stohl, A., Trainer, M., Thompson, A., Witte, J. C., Oltmans, S. J., Johnson,
1092 B. J., Merrill, J., Moody, J. L., Tarasick, D., Néédéc, P., Forbes, G., Newchurch, M. J.,
1093 Schmidlin, F. J., Johnson, B. J., Turquety, S., Baughcum, S. L., Ren, X., Fehsenfeld, F. C.,
1094 Meagher, J. F., Spichtinger, N., Brown, C. C., McKeen, S. A., McDermid, I. S., and

1095 Leblanc, T.: Large upper tropospheric ozone enhancements above mid-latitude North
1096 America during summer: in situ evidence from the IONS and MOZAIC ozone
1097 monitoring network, *J. Geophys. Res.*, 111, D24S05, doi:10.1029/2006JD007306, 2006.
1098

1099 Cristofanelli, P., Bonasoni, P., Collins, W., Feichter, J., Forster, C., James, P., Kentarchos,
1100 A., Kubik, P. W., Land, C., Meloen, J., Roelofs, G. J., Siegmund, P., Sprenger, M.,
1101 Schnabel, C., Stohl, A., Tobler, L., Tositti, L., Trickl, T., and Zanis, P.:
1102 Stratosphere-to-troposphere transport: a model and method evaluation, STACCATO
1103 special section of *J. Geophys. Res.*, 108, 8525, doi:10.1029/2002JD002600, 2003.
1104

1105 Daley, R.: *Atmospheric Data Analysis*, Cambridge University Press, Cambridge, 1991.
1106

1107 Damoah, R., Spichtinger, N., Forster, C., James, P., Mattis, I., Wandinger, U., Beirle, S.,
1108 Wagner, T., and Stohl, A.: Around the world in 17 days - hemispheric-scale transport of
1109 forest fire smoke from Russia in May 2003, *Atmos. Chem. Phys.*, 4, 1311-1321,
1110 doi:10.5194/acp-4-1311-2004, 2004.
1111

1112 Davies, D. K., Ilavajhala, S., Wong, M. M., and Justice, C. O.: Fire information for
1113 resource management system: archiving and distributing MODIS active fire data, *IEEE T.*
1114 *Geosci. Remote*, 47,72-79, 2009.
1115

1116 Deeter, M. N., Emmons, L. K., Francis, G. L., Edwards, D. P., Gille, J. C., Warner, J. X.,
1117 Khattatov, B., Ziskin, D., Lamarque, J.-F., Ho, S.-P., Yudin, V., Attié J.-L., Packman, D.,
1118 Chen, J., Mao, D., and Drummond, J. R.: Operational carbon monoxide retrieval
1119 algorithm and selected results for the MOPITT instrument, *J. Geophys. Res.*, 108, 4399,
1120 doi:10.1029/2002JD003186, 2003.
1121

1122 Deeter, M. N., Emmons, L. K., Edwards, D. P., Gille, J. C., and Drummond, J. R.:
1123 Vertical resolution and information content of CO profiles retrieved by MOPITT,
1124 *Geophys. Res. Lett.*, 31, L15112, doi:10.1029/2004GL020235, 2004.
1125

1126 Deeter, M. N., Worden, H. M., Edwards, D. P., Gille, J. C., and Andrews, A. E.:
1127 Evaluation of MOPITT retrievals of lower-tropospheric carbon monoxide over the United
1128 States, *J. Geophys. Res.*, 117, D13306, doi:10.1029/2012JD017553, 2012.
1129

1130 [Deeter, M. N., Martínez-Alonso, S., Edwards, D. P., Emmons, L. K., Gille, J. C., Worden,](#)
1131 [H. M., Pittman, J. V., Daube, B. C., and Wofsy, S. C.: Validation of MOPITT Version 5](#)
1132 [thermal-infrared, near-infrared, and multispectral carbon monoxide profile retrievals for](#)
1133 [2000–2011, *J. Geophys. Res.*, doi:10.1002/jgrd.50272, 2013.](#)
1134

1135 Dickerson, R. R., Huffman, G. J., Luke, W. T., Nunnermacker, L. J., Pickering, K. E.,
1136 Leslie, A. C. D., Lindsey, C. G., Slinn, W. G. N., Kelly, T. J., Daum, P. H., Delany, A. C.,
1137 Greenberg, J. P., Zimmerman, P. R., Boatman, J. F., Ray, J. D., and Stedman, D. H.:
1138 Thunderstorms – an important mechanism in the transport of air pollutants, *Science*, 235,
1139 4787, 460-464, 1987.
1140

1141 Dickerson, R. R., Li, C., Li, Z., Marufu, L., T., Stehr, J. W., McClure, B., Krotkov, N.,
1142 Chen, H., Wang, P., Xia, X., Ban, X., Gong, F., Yuan, J., and Yang, J.: Aircraft
1143 observations of dust and pollutants over northeast China: insight into the meteorological
1144 mechanisms of transport, *J. Geophys. Res.*, 112, D24S90, doi:10.1029/2007JD008999,
1145 2007.

1146
1147 Ding, A., Wang, T., Xue, L., Gao, J., Stohl, A., Lei, H., Jin, D., Ren, Y., Wang, X., Wei, X.,
1148 Qi, Y., Liu, J., and Zhang, X.: Transport of north China air pollution by midlatitude
1149 cyclones: case study of aircraft measurements in summer 2007, *J. Geophys. Res.*, 114,
1150 D08304, doi:10.1029/2008JD011023, 2009.

1151
1152 Donnell, E. A., Fish, D. J., Dicks, E. M., and Thorpe, A. J.: Mechanisms for pollutant
1153 transport between the boundary layer and the free troposphere, *J. Geophys. Res.*, 106,
1154 7847-7856, 2001.

1155
1156 Drummond, J. R.: Measurements of pollution in the troposphere (MOPITT), in: *The Use*
1157 *of EOS for Studies of Atmospheric Physics*, edited by: Gille, J. C. and Visconti, G., North
1158 Holland, New York, 77-101, 1992.

1159
1160 Drummond, J. R. and Mand, G. S.: The measurements of pollution in the troposphere
1161 (MOPITT) instrument: overall performance and calibration requirements, *J. Atmos.*
1162 *Ocean. Tech.*, 13, 314-320, ~~1996~~.
1163 [1996](#).

1164
1165 Duncan, B. N., Martin, R. V., Staudt, A. C., Yevich, R., and Logan, J. A.: Interannual and
1166 seasonal variability of biomass burning emissions constrained by satellite observations, *J.*
1167 *Geophys. Res.*, 108, 4040, doi:10.1029/2002JD002378, 2003.

1168
1169 Duncan, B. N., Logan, J. A., Bey, I., Megretskaia, I. A., Yantosca, R. M., Novelli, P. C.,
1170 Jones, N. B., and Rinsland, C. P.: Global budget of CO, 1988-1997: source estimates and
1171 validation with a global model, *J. Geophys. Res.*, 112, D22301,
1172 doi:10.1029/2007JD008459, 2007.

1173
1174 Eckhardt, S., Stohl, A., Wernli, H., James, P., Forster, C., and Spichtinger, N.: A 15-Year
1175 climatology of warm conveyor belts, *J. Climate*, 17, 218-237, 2004.

1176
1177 Edwards, D. P., Halvorson, C. M., and Gille, J. C.: Radiative transfer modeling for the
1178 EOS Terra satellite measurements of pollution in the troposphere (MOPITT instrument), *J.*
1179 *Geophys. Res.*, 104, 16755-16775, 1999.

1180
1181 Emmons, L. K., Deeter, M. N., Gille, J. C., Edwards, D. P., Attie, J.-L., Warner, J., Ziskin,
1182 D., Khattatov, B., Yudin, V., Lamarque, J.-F., Ho, S.-P., Mao, D., Chen, J. S., Drummond,
1183 J., Novelli, P., Sachse, G., Coffey, M. T., Hannigan, J. W., Gerbig, C., Kawakami, S.,
1184 Kondo, Y., Takegawa, N., Baehr, J., and Ziereis, H.: Validation of MOPITT CO retrievals
1185 with aircraft in situ profiles, *J. Geophys. Res.*, 109, D03309, doi:10.1029/2003JD004101,
1186 2004.

1187
1188 Giglio, L., Descloitres, J., Justice, C. O., and Kaufman, Y. J.: An enhanced contextual fire
1189 detection algorithm for MODIS, *Remote Sens. Environ.*, 87, 273-282, 2003.
1190
1191 Hao, H., Valks, P., Loyola, D., Chen, Y. F., and Zimmer, W.: Space-based measurements
1192 of air quality during the World Expo 2010 in Shanghai, *Environ. Res. Lett.*, 6, 044004,
1193 doi:10.1088/1748-9326/6/4/044004, 2011.
1194
1195 He, H., Tarasick, D. W., Hocking, W. K., Carey-Smith, T. K., Rochon, Y., Zhang, J.,
1196 Makar, P. A., Osman, M., Brook, J., Moran, M. D., Jones, D. B. A., Mihele, C., Wei, J. C.,
1197 Osterman, G., Argall, P. S., McConnell, J., and Bourqui, M. S.: Transport analysis of
1198 ozone enhancement in Southern Ontario during BAQS-Met, *Atmos. Chem. Phys.*, 11,
1199 2569-2583, doi:10.5194/acp-11-2569-2011, 2011.
1200
1201 Heald, C. L., Jacob, D. J., Fiore, A. M., Emmons, L. K., Gille, J. C., Deeter, M. N.,
1202 Warner, J., Edwards, D. P., Crawford, J. H., Hamlin, A. J., Sachse, G. W., Browell, E. V.,
1203 Avery, M. A., Vay, S. A., Westberg, D. J., Blake, D. R., Singh, H. B., Sandholm, S. T.,
1204 Talbot, R. W., and Fuelberg, H. E.: Asian outflow and transpacific transport of carbon
1205 monoxide and ozone pollution: an integrated satellite, aircraft and model perspective, *J.*
1206 *Geophys. Res.*, 108, 4804, doi:10.1029/2003JD003507, 2003.
1207
1208 Hocking, W. K., Carey-Smith, T. K., Tarasick, D. W., Argall, P. S., Strong, K., Rochon, Y.,
1209 Zawadzki, I., and Taylor, P. A.: Detection of stratospheric ozone intrusion by wind
1210 profiler radars, *Nature*, 450, 281-284, doi:10.1038/nature06312, 2007.
1211
1212 Holloway, T., Levy II, H., and Kasibhatla, P.: Global distribution of carbon monoxide, *J.*
1213 *Geophys. Res.*, 105, 12123-12147, doi:10.1029/1999JD901173, 2000.
1214
1215 Jacob, D. J.: *Introduction to Atmospheric Chemistry*, Princeton University Press,
1216 Princeton, New Jersey, 1999.
1217
1218 Jacob, D. J., Crawford, J. H., Kleb, M. M., Connors, V. S., Bendura, R. J., Raper, J. L.,
1219 Sachse, G. W., Gille, J. C., Emmons L., and Heald, C. L.: Transport and Chemical
1220 Evolution over the Pacific (TRACE-P) aircraft mission: design, execution, and first
1221 results, *J. Geophys. Res.*, 108, 9000, doi:10.1029/2002JD003276, 2003.
1222
1223 Jaffe, D., Anderson, T., Covert, D., Kotchenruther, R., Trost, B., Danielson, J., Simpson,
1224 W., Berntsen, T., Karlsdottir, S., Blake, D., Harris, J., Carmichael, G., and Uno, I.:
1225 Transport of Asian air pollution to North America, *Geophys. Res. Lett.*, 26, 711-714,
1226 1999.
1227
1228 Jaffe, D., Bertschi, I., Jaegle, L., Novelli, P., Reid, J. S., Tanimoto, H., Vingarzan, R., and
1229 Westphal, D. L.: Long-range transport of Siberian biomass burning emissions and impact
1230 on surface ozone in western North America, *Geophys. Res. Lett.*, 31, L16106,
1231 doi:10.1029/2004GL020093, 2004.
1232

1233 Jiang, Z., Jones, D. B. A., Kopacz, M., Liu, J., Henze, D. K., and Heald, C.: Quantifying
1234 the impact of model errors on top-down estimates of carbon monoxide emissions using
1235 satellite observations, *J. Geophys. Res.* 116, D15306, doi:10.1029/2010JD015282, 2011.
1236

1237 Jones, D. B. A., Bowman, K. W., Logan, J. A., Heald, C. L., Liu, J., Luo, M., Worden, J.,
1238 and Drummond, J.: The zonal structure of tropical O₃ and CO as observed by the
1239 Tropospheric Emission Spectrometer in November 2004 - Part 1: Inverse modeling of CO
1240 emissions, *Atmos. Chem. Phys.*, 9, 3547-3562, doi:10.5194/acp-9-3547-2009, 2009.
1241

1242 Justice, C. O., Giglio, L., Korontzi, S., Owens, J., Morisette, J. T., Roy, D., Descloitres, J.,
1243 Alleaume, S., Petitcolin, F., and Kaufman, Y.: The MODIS fire products, *Remote Sens.*
1244 *Environ.*, 83, 244-262, 2002.
1245

1246 Kar, J., Bremer, H., Drummond, J. R., Rochon, Y. J., Jones, D. B. A., Nichitiu, F., Zou, J.,
1247 Liu, J., Gille, J. C., Edwards, D. P., Deeter, M. N., Francis, G., Ziskin, D., and Warner, J.:
1248 Evidence of vertical transport of carbon monoxide from measurements of pollution in the
1249 troposphere (MOPITT). *Geophys. Res. Lett.*, 31, L23105, doi:10.1029/2004GL021128,
1250 2004.
1251

1252 Kar, J., Drummond, J. R., Jones, D. B. A., Liu, J., Nichitiu, F., Zou, J., Gille, J. C.
1253 Edwards, D. P., Deeter, M. N.: Carbon monoxide (CO) maximum over the Zagros
1254 mountains in the Middle East: signature of mountain venting?, *Geophys. Res. Lett.*, 33,
1255 L15819, doi:10.1029/2006GL026231, 2006.
1256

1257 Kar, J., Jones, D. B. A., Drummond, J. R., Attie, J. L., Liu, J., Zou, J., Nichitiu, F.,
1258 Seymour, M. D., Edwards, D. P., Deeter, M. N., Gille, J. C., and Richter, A.:
1259 Measurement of low-altitude CO over the Indian subcontinent by MOPITT, *J. Geophys.*
1260 *Res.*, 113, D16307, doi:10.1029/2007JD009362, 2008.
1261

1262 Kopacz, M., Jacob, D. J., Fisher, J. A., Logan, J. A., Zhang, L., Megretskaja, I. A.,
1263 Yantosca, R. M., Singh, K., Henze, D. K., Burrows, J. P., Buchwitz, M., Khlystova, I.,
1264 McMillan, W. W., Gille, J. C., Edwards, D. P., Eldering, A., Thouret, V., and Nédélec, P.:
1265 Global estimates of CO sources with high resolution by adjoint inversion of multiple
1266 satellite datasets (MOPITT, AIRS, SCIAMACHY, TES), *Atmos. Chem. Phys.*, 10,
1267 855-876, doi:10.5194/acp-10-855-2010, 2010.
1268

1269 Kowol-Santen, J., Beekmann, M., Schmitgen, S., and Dewey, K.: Tracer analysis of
1270 transport from the boundary layer to the free atmosphere, *Geophys. Res. Lett.*, 28,
1271 2907-2910, 2001.
1272

1273 Lavoué D., Lioussé, C., Cachier, H., Stocks, B. J., and Goldammer, J. G.: Modeling of
1274 carbonaceous particles emitted by boreal and temperate wildfires at northern latitudes, *J.*
1275 *Geophys. Res.*, 105, 26871-26890, doi:10.1029/2000JD900180, 2000.
1276

1277 Lawrence, M. G., Rasch, P. J., von Kuhlmann, R., Williams, J., Fischer, H., de Reus, M.,
1278 Lelieveld, J., Crutzen, P. J., Schultz, M., Stier, P., Huntrieser, H., Heland, J., Stohl, A.,

1279 Forster, C., Elbern, H., Jakobs, H., and Dickerson, R. R.: Global chemical weather
1280 forecasts for field campaign planning: predictions and observations of large-scale features
1281 during MINOS, CONTRACE, and INDOEX, *Atmos. Chem. Phys.*, 3, 267-289,
1282 doi:10.5194/acp-3-267-2003, 2003.
1283

1284 Li, Q. B., Jacob, D. J., Park, R. J., Wang, Y. X., Heald, C. L., Hudman, R., Yantosca, R.
1285 M., Martin, R. V., and Evans, M. J.: North American pollution outflow and the trapping
1286 of convectively lifted pollution by upper-level anticyclone, *J. Geophys. Res.*, 110,
1287 D10301, doi:10.1029/2004JD005039, 2005.
1288

1289 Li, Z., Chen, H., Cribb, M., Dickerson, R., Holben, B., Li, C., Lu, D., Luo, Y., Maring, H.,
1290 Shi, G., Tsay, S.-C., Wang, P., Wang, Y., Xia, X., Zheng, Y., Yuan, T., and Zhao, F.:
1291 Preface to special section on East Asian Studies of Tropospheric Aerosols: an
1292 International Regional Experiment (EAST-AIRE), *J. Geophys. Res.*, 112, D22S00,
1293 doi:10.1029/2007JD008853, 2007.
1294

1295 Liang, Q., Jaegle, L., Jaffe, D. A., Weiss-Penzias, P., Heckman, A., and Snow, J. A.:
1296 Long-range transport of Asian pollution to the northeast Pacific: seasonal variations and
1297 transport pathways of carbon monoxide, *J. Geophys. Res.*, 109, D23S07,
1298 doi:10.1029/2003JD004402, 2004.
1299

1300 Lin, C.-Y., Hsu, H.-m., Lee, Y. H., Kuo, C. H., Sheng, Y.-F., and Chu, D. A.: A new
1301 transport mechanism of biomass burning from Indochina as identified by modeling
1302 studies, *Atmos. Chem. Phys.*, 9, 7901-7911, doi:10.5194/acp-9-7901-2009, 2009.
1303

1304 Liu, C., Beirle, S., Butler, T., Liu, J., Hoor, P., Jöckel, P., Penning de Vries, M., Pozzer, A.,
1305 Frankenberg, C., Lawrence, M. G., Lelieveld, J., Platt, U., and Wagner, T.: Application of
1306 SCIAMACHY and MOPITT CO total column measurements to evaluate model results
1307 over biomass burning regions and Eastern China, *Atmos. Chem. Phys.*, 11, 6083-6114,
1308 doi:10.5194/acp-11-6083-2011, 2011.
1309

1310 Liu, H. Y., Jacob, D. J., Bey, I., Yantosca, R. M., Duncan, B. N., and Sachse, G.W.:
1311 Transport pathways for Asian combustion outflow over the Pacific: interannual and
1312 seasonal variations, *J. Geophys. Res.*, 108, 8786, doi:10.1029/2002JD003102, 2003.
1313

1314 Liu, J., Drummond, J. R., Li, Q., Gille, J. C., and Ziskin, D. C.: Satellite mapping of CO
1315 emission from forest fires in northwest America using MOPITT measurements, *Remote
1316 Sens. Environ.*, 95, 502-516, 2005.
1317

1318 Liu, J., Drummond, J. R., Jones, D. B. A., Cao, Z., Bremer, H., Kar, J., Zou, J., Nichitiu,
1319 F., and Gille, J. C.: Large horizontal gradients in atmospheric CO at the synoptic scale as
1320 seen by spaceborne measurements of pollution in the troposphere, *J. Geophys. Res.*, 111,
1321 D02306, doi:10.1029/2005JD006076, 2006.
1322

1323 Mari, C., Evans, M. J., Palmer, P. I., Jacob, D. J., and Sachse, G. W.: Export of Asian
1324 pollution during two cold front episodes of the TRACE-P experiment, *J. Geophys. Res.*,

1325 109, D15S17, doi:10.1029/2003JD004307, 2004.
1326
1327 Miyazaki, Y., Kondo, Y., Koike, M., Fuelberg, H. E., Kiley, C. M., Kita, K., Takegawa, N.,
1328 Sachse, G. W., Flocke, F., Weinheimer, A. J., Singh, H. B., Eisele, F. L., Zondlo, M.,
1329 Talbot, R. W., Sandholm, S. T., Avery, M. A., and Blake, D. R.: Synoptic-scale transport
1330 of reactive nitrogen over the western Pacific in spring, *J. Geophys. Res.*, 108, 8788,
1331 doi:10.1029/2002JD003248,2003.
1332
1333 Marenco, A., Thouret, V., Nédélec, P., Smit, H., Helten, M., Kley, D., Karcher, F., Simon,
1334 P., Law, K., Pyle, J., Poschmann, G., Wrede, R. V., Hume, C., and Cook, T: Measurement
1335 of ozone and water vapor by Airbus in-service aircraft: the MOZAIC airborne program,
1336 An overview, *J. Geophys. Res.*, 103, 25631-25642, 1998.
1337
1338 Nassar, R., Logan, J. A., Megretskaia, I. A., Murray, L. T., Zhang, L., and Jones, D. B. A.:
1339 Analysis of tropical tropospheric ozone, carbon monoxide, and water vapor during the
1340 2006 El Niño using TES observations and the GEOS-Chem model, *J. Geophys. Res.*, 114,
1341 D17304, doi:10.1029/2009JD011760, 2009.
1342
1343 Nassar, R., Jones, D. B. A., Suntharalingam, P., Chen, J. M., Andres, R. J., Wecht, K. J.,
1344 Yantosca, R. M., Kulawik, S. S., Bowman, K. W., Worden, J. R., Machida, T., and
1345 Matsueda, H.: Modeling global atmospheric CO₂ with improved emission inventories and
1346 CO₂ production from the oxidation of other carbon species, *Geosci. Model Dev.*, 3,
1347 689-716, doi:10.5194/gmd-3-689-2010, 2010.
1348
1349 Nédélec, P., Thpuret, V., Brioude, J., Sauvage, B., Cammas, J., Stohl, A.: Extreme CO
1350 concentrations in the upper troposphere over northeast Asia in June 2003 from the in situ
1351 MOZAIC aircraft data, *Geophys. Res. Lett.*, 32, L14807, doi:10.1029/2005GL023141,
1352 2005.
1353
1354 Novelli, P., Masarie, K. A., and Lang, P. M.: Distributions and recent changes of carbon
1355 monoxide in the lower troposphere, *J. Geophys. Res.*, 103, 19015 - 19033, 1998.
1356
1357 Olivier, J. G. J. and Berdowski, J. J. M.: Global emission sources and sinks, in: *The*
1358 *Climate System*, edited by: Berdowski, J., Guicherit, R., and Heij, B. J., Swets &
1359 Zeitlinger, Lisse, the Netherlands, 33 -77, 2001.
1360
1361 Oltmans, S. J., Lefohn, A. S., Harris, J. M., Tarasick, D. W., Thompson, A. M.,
1362 Wernli, H., Johnson, B. J., Novelli, P. C., Montzka, S. A., Ray, J. D., Patrick, L. C.,
1363 Sweeney, C., Jefferson, A., Dann, T., Davies, J., Shapiro, M., Holben, B. N.: Enhanced
1364 ozone over western North America from biomass burning in Eurasia during April 2008 as
1365 seen in surface and profile observations, *Atmos. Environ.*, 44, 4497-4509, 2010.
1366
1367 Pan, L., Gille, J. C., Edwards, D. P., Bailey, P. L., and Rodgers, C. D.: Retrieval of
1368 tropospheric carbon monoxide for the MOPITT experiment, *J. Geophys. Res.*, 103,
1369 32277-32290, 1998.
1370

1371 Pickering, K. E., Dickerson, R. R., Huffman, G. J., Boatman, J. F., and Schanot, A.: Trace
1372 gas transport in the vicinity of frontal convective clouds, *J. Geophys. Res.*, 93, 759 -773,
1373 doi:10.1029/JD093iD01p00759, 1998.
1374

1375 Randel, W. J., Park, M., Emmons, L., Kinnison, D., Bernath, P., Walker, K. A., Boone, C.,
1376 and Pumphrey, H.: Asian monsoon transport of pollution to the stratosphere, *Science*, 328,
1377 611-613, doi:10.1126/science.1182274, 2010.
1378

1379 Rogers, C. D.: *Inverse Methods for Atmospheric Sounding, Theory and Practice*, World
1380 Sci., River Edge, N.J., 2000.
1381

1382 Schultz, M. G.: On the use of ATSR fire count data to estimate the seasonal and
1383 interannual variability of vegetation fire emissions, *Atmos. Chem. Phys.*, 2, 387-395,
1384 doi:10.5194/acp-2-387-2002, 2002.
1385

1386 Stohl, A.: A 1-year Lagrangian "climatology" of airstreams in the North Hemisphere
1387 troposphere and lowermost stratosphere, *J. Geophys. Res.*, 106, 7263-7279, 2001.
1388

1389 Stohl, A., Hittenberger, M., and Wotawa, G.: Validation of the Lagrangian particle
1390 dispersion model FLEXPART against large scale tracer experiment data, *Atmos. Environ.*,
1391 24, 4245-4264, 1998.
1392

1393 Stohl, A., Eckhardt, S., Forster, C., James, P., and Spichtinger, N.: On the pathways and
1394 timescales of intercontinental air pollution transport, *J. Geophys. Res.*, 107, 4684,
1395 doi:10.1029/2001JD001396, 2002.
1396

1397 Stohl, A., Forster, C., Frank, A., Seibert, P., and Wotawa, G.: Technical note: The
1398 Lagrangian particle dispersion model FLEXPART version 6.2, *Atmos. Chem. Phys.*, 5,
1399 2461-2474, doi:10.5194/acp-5-2461-2005, 2005.
1400

1401 Streets, D. G., Zhang, Q., Wang, L., He, K., Hao, J., Wu, Y., Tang, Y., and Carmichael, G.
1402 R.: Revisiting China's CO emissions after the Transport and Chemical Evolution over the
1403 Pacific (TRACE-P) mission: synthesis of inventories, atmospheric modeling, and
1404 observations, *J. Geophys. Res.*, 111, D14306, doi:10.1029/2006JD007118, 2006.
1405

1406 Su, M., Lin, Y., Fan, X., Peng, L., Zhao, C.: Impacts of global emissions of CO, NO_x, and
1407 CH₄ on China tropospheric hydroxyl free radicals, *Adv. Atmos. Sci.*, 29, 4, 838-854,
1408 2012.
1409

1410 Suntharalingam, P., Jacob, D. J., Palmer, P. I., Logan, J. A., Yantosca, R. M., Xiao, Y.,
1411 Evans, M. J., Streets, D., Vay, S. A., and Sachse, G.: Improved quantification of Chinese
1412 carbon fluxes using CO₂/CO correlations in Asian outflow, *J. Geophys. Res.*, 109,
1413 D18S18, doi:10.1029/2003JD004362, 2004.
1414

1415 Tao, S. and Ding, Y.: Observational evidence of the influence of the Qinghai-Xizang
1416 (Tibet) Plateau on the occurrence of heavy rain and severe convective storms in China, B.

1417 Am. Meteorol. Soc., 62, 2-30, 1981.
1418
1419 Tanimoto, H., Sawa, Y., Yonemura, S., Yumimoto, K., Matsueda, H., Uno, I., Hayasaka,
1420 T., Mukai, H., Tohjima, Y., Tsuboi, K., and Zhang, L.: Diagnosing recent CO emissions
1421 and ozone evolution in East Asia using coordinated surface observations, adjoint inverse
1422 modeling, and MOPITT satellite data, *Atmos. Chem. Phys.*, 8, 3867-3880,
1423 doi:10.5194/acp-8-3867-2008, 2008.
1424
1425 Tsutsumi, Y., Makino, Y., and Jensen, J. B.: Vertical and latitudinal distributions of
1426 tropospheric ozone over the western Pacific: case studies from the PACE aircraft
1427 missions, *J. Geophys. Res.*, 108, 4251, doi:10.1029/2001JD001374, 2003.
1428
1429 van der Werf, G. R., Randerson, J. T., Giglio, L., Collatz, G. J., Mu, M., Kasibhatla, P. S.,
1430 Morton, D. C., DeFries, R. S., Jin, Y., and van Leeuwen, T. T.: Global fire emissions and
1431 the contribution of deforestation, savanna, forest, agricultural, and peat fires (1997-2009),
1432 *Atmos. Chem. Phys.*, 10, 11707--11735, doi:10.5194/acp-10-11707-2010, 2010.
1433
1434 Wang, T., Nie, W., Gao, J., Xue, L. K., Gao, X. M., Wang, X. F., Qiu, J., Poon, C. N.,
1435 Meinardi, S., Blake, D., Wang, S. L., Ding, A. J., Chai, F. H., Zhang, Q. Z., and Wang, W.
1436 X.: Air quality during the 2008 Beijing Olympics: secondary pollutants and regional
1437 impact, *Atmos. Chem. Phys.*, 10, 7603-7615, doi:10.5194/acp-10-7603-2010, 2010.
1438
1439 Wang, X. L., Feng, Y., Compo, G. P., Swail, V. R., Zwiers, F. W., Allan, R. J., and
1440 Sardeshmukh, P. D.: Trends and low frequency variability of extra-tropical cyclone
1441 activity in the ensemble of twentieth century reanalysis, *Clim. Dynam.*, 40, 2775-2800,
1442 doi:10.1007/s00382-012-1450-9, 2013.
1443
1444 [Wofsy, S. C., and the HIPPO Science Team and Cooperating Modellers and Satellite](#)
1445 [Teams: HIAPER pole-to-pole observations \(HIPPO\): Fine-grained, global-scale](#)
1446 [measurements of climatically important atmospheric gases and aerosols, *Phil. Trans. R.*](#)
1447 [Soc. A, 369, 2073–2086, doi:10.1098/rsta.2010.0313, 2011.](#)
1448
1449 Worden, H. M., Deeter, M. N., Edwards, D. P., Gille, J. C., Drummond, J. R., and
1450 Nédélec, P.: Observations of near-surface carbon monoxide from space using MOPITT
1451 multispectral retrievals, *J. Geophys. Res.*, 115, D18314, doi:10.1029/2010JD014242,
1452 2010.
1453
1454 Wotawa, G., Novelli, P. C., Trainer, M., and Granier, C.: Interannual variability of
1455 summertime CO concentrations in the Northern Hemisphere explained by boreal forest
1456 fires in North America and Russia, *Geophys. Res. Lett.*, 28, 4575-4578, 2001.
1457
1458 Yienger, J. J., Galanter, M., Holloway, T. A., Phadnis, M. J., Guttikunda, S. K.,
1459 Carmichael, G. R., Moxim, W. J., and Levy II, H.: The episodic nature of air pollution
1460 transport from Asia to North America, *J. Geophys. Res.*, 105, 26931-26945,
1461 doi:10.1029/2000JD900309, 2000.
1462

1463 Yu, R., Xu, Y., Zhou, T., and Li, J.: Relation between rainfall duration and diurnal
1464 variation in the warm season precipitation over central eastern China, *Geophys. Res. Lett.*,
1465 34, L13703, doi:10.1029/2007GL030315, 2007.

1466
1467 Yue, X. and Wang, H.: The springtime North Asia cyclone activity index and the
1468 Southern Annular Mode, *Adv. Atmos. Sci.*, 25, 673-679, 2008.

1469
1470 Yurganov, L. N., McMillan, W. W., Dzhola, A. V., Grechko, E. I., Jones, N. B., and van
1471 der Werf, G.: Global AIRS and MOPITT CO measurements: validation, comparison, and
1472 links to biomass burning variations and carbon cycle, *J. Geophys. Res.*, 113, D09301,
1473 doi:10.1029/2007JD009229, 2008.

1474
1475 Zhang, L., Jacob, D. J., Bowman, K. W., Logan, J. A., Turquety, S., Hudman, R. C., Li, Q.
1476 B., Beer, R., Worden, H. M., Worden, J. R., Rinsland, C. P., Kulawik, S. S., Lampel, M.
1477 C., Shephard, M. W., Fisher, B. M., Eldering, A., and Avery, M. A.: Ozone-CO
1478 correlations determined by the TES satellite instrument in continental outflow regions,
1479 *Geophys. Res. Lett.*, 33, L18804, doi:10.1029/2006GL026399, 2006.

1480
1481 Zhang, Q., Streets, D. G., Carmichael, G. R., He, K. B., Huo, H., Kannari, A., Klimont, Z.,
1482 Park, I. S., Reddy, S., Fu, J. S., Chen, D., Duan, L., Lei, Y., Wang, L. T., and Yao, Z. L.:
1483 Asian emissions in 2006 for the NASA INTEX-B mission, *Atmos. Chem. Phys.*, 9,
1484 5131-5153, doi:10.5194/acp-9-5131-2009, 2009.

1485
1486 Zhao, C., Wang, W., Yang, Y., Fu, R., Cunnold, D., and Choi, Y.: Impact of East Asian
1487 summer monsoon on the air quality over China: view from space, *J. Geophys. Res.*, 115,
1488 D09301, doi:10.1029/2009JD012745, 2010.

1489
1490 Zhao, T. L., Gong, S. L., Zhang, X. Y., and Jaffe, D. A.: Asian dust storm influence on
1491 North American ambient PM levels: observational evidence and controlling factors,
1492 *Atmos. Chem. Phys.*, 8, 2717-2728, doi:10.5194/acp-8-2717-2008, 2008.

1493
1494 Zhou, D., Ding, A., Mao, H., Fu, C., Wang, T., Chan, L. Y., Ding, K., Zhang, Y., Liu, J.,
1495 Lu, A., and Hao, N.: Impacts of the East Asian monsoon on lower tropospheric ozone
1496 over coastal South China, *Environ. Res. Lett.*, 8, 044011,
1497 doi:10.1088/1748-9326/8/4/044011, 2013.

1498
1499